SENSE: SENSING SIMILARITY SEEING STRUCTURE

Anonymous authorsPaper under double-blind review

ABSTRACT

Dimensionality reduction is widely used to visualize and analyze high-dimensional data, but most methods assume centralized access to all pairwise similarities, which is infeasible in privacy-sensitive, decentralized settings. We introduce **SENSE**, a geometry-aware framework for privacy-preserving decentralized representation learning. SENSE reconstructs global structure from sparse, locally observed distances via structured matrix completion, requiring no raw data sharing or iterative communication. It supports both Euclidean and hyperbolic geometries, adapts to flat and hierarchical structures, and operates under four deployment regimes reflecting real-world data availability. By design, SENSE safeguards raw features while producing faithful embeddings. Our theoretical analysis establishes formal privacy guarantees, and experiments on diverse benchmark datasets show that SENSE matches centralized baselines while remaining efficient and privacy-preserving. Our code is publicly available here.

1 Introduction

Dimensionality reduction (DR) projects high-dimensional data into lower-dimensional spaces where patterns are easier to interpret (Jolliffe & Cadima, 2016). A prominent family is neighbor embedding (NE) methods, which preserve local similarity relationships (Sorzano et al., 2014). Notable examples include t-SNE (van der Maaten & Hinton, 2008) and UMAP (McInnes et al., 2020), widely used in visualization (Cavallo & Demiralp, 2018), anomaly detection (Sadr et al., 2019), and exploratory analysis (Ding et al., 2002). Contrastive Neighbor Embedding (CNE) (Damrich et al., 2023) extends these ideas by casting neighborhood preservation into a contrastive learning framework that emphasizes the role of negatives. In contrast, PHATE (Moon et al., 2019) departs from NE altogether, leveraging diffusion geometry to capture both local and global structures. Together, these methods illustrate the diversity and impact of modern DR. However, most similarity-based DR approaches assume centralized access to all pairwise similarities, a condition rarely met in practice. In domains from healthcare and finance to IoT and social media, data are distributed across clients under strict privacy and communication constraints (Dwork et al., 2014; McMahan et al., 2017; Qiao et al., 2023), leaving inter-client similarities inaccessible. This fragmented view of the data yields embeddings that misrepresent relationships and fail to preserve the underlying structure (Li et al., 2024).

Related Work. Several approaches have addressed these challenges but are constrained by scalability, privacy, or deployment practicality. SMAP (Xia et al., 2020) offers strong privacy via Secure Multi-party Computation (SMC), but its cryptographic overhead makes large-scale use infeasible and prevents support for methods like UMAP. FedNE (Li et al., 2024) allows federated NE but lacks intrinsic privacy, relies on heavy server-client interaction, and is vulnerable to inversion attacks. Fed-tSNE and Fed-UMAP (Qiao et al., 2024) generate synthetic anchors via MMD alignment but assume multi-sample clients, fail in single-sample regimes, and remain susceptible to adversarial corruption. These limitations call for frameworks that are communication-efficient, privacy-preserving, and yield faithful embeddings. To this end, we propose SENSE, a geometry-aware framework for decentralized representation learning. It supports both Euclidean and hyperbolic spaces, the latter crucial for capturing hierarchical structures in domains such as social and biological networks (Malik et al., 2025). At its core, SENSE reconstructs global structure from sparse local distances, avoiding raw data sharing, iterative communication, or centralized storage. The completed distance matrix is then used with classical NE methods, CNE, PHATE, or hyperbolic CoSNE (Guo et al., 2022), enabling scalable and privacy-preserving embeddings in decentralized environments.

The discussion so far has emphasized privacy as a key barrier to decentralized representation learning, but this naturally raises a deeper question: what do we actually mean by privacy? The term is

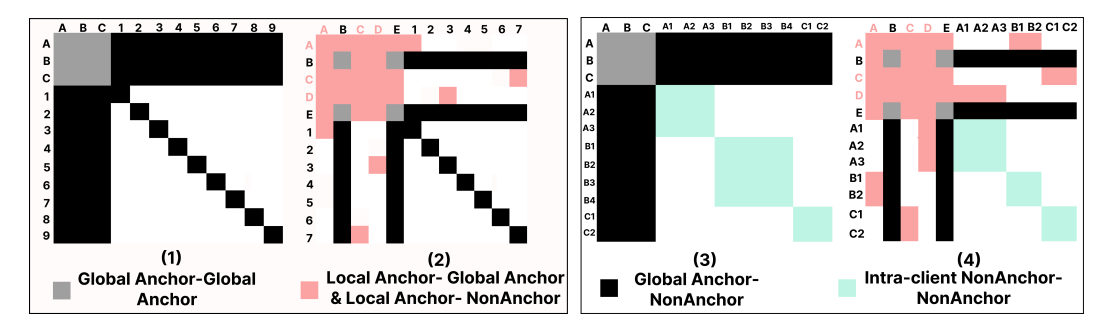


Figure 1: Observed entries in the global distance matrix D under four SENSE configurations: (1) *Pointwise-Full*, (2) *Pointwise-Partial*, (3) *Multisite-Full*, and (4) *Multisite-Partial*. Configurations differ by visibility of Anchor–NonAnchor (A–NA) and NA–NA blocks, determined by client data locality and anchor access. In *Pointwise*, each client contributes a single NA (e.g., 1, 2, ..., 9), whereas *Multisite* allows intra-client NA–NA observations (e.g., A1, A2, ..., C2). *Full* modes grant all NAs access to the global anchor set (e.g., A–E), yielding complete A–NA blocks, while *Partial* modes restrict clients to disjoint anchor subsets, producing sparse structured observations.

inherently contextual. Across domains such as healthcare, finance, and social platforms, data often encode highly sensitive attributes such as medical records, geolocation traces, genomic records, financial transactions, and social interactions (Dwork et al., 2014; Rieke et al., 2020; Byrd & Polychroniadou, 2020; Lim et al., 2020). Over the years, privacy has been formalized in diverse ways, from cryptographic guarantees to statistical indistinguishability and database anonymity, reflecting that there is no single universal notion, only definitions shaped by the threat model and application context (Yao, 1982; Goldreich, 1998; Dwork et al., 2006; Abadi et al., 2016; Sweeney, 2002; Kairouz et al., 2021). So, what does privacy mean in our setting?

In SENSE, clients may typically hold sensitive datasets, such as patient health records, demographic attributes, or financial profiles, making the raw feature vectors $\{x_i\}$ the sensitive objects. Disclosing such data would be a severe violation. Instead, SENSE relies on distances to some anchor points as safe coordination signals, reconstructing inter-client similarity (i.e., who is close to whom) without exposing raw features, thereby producing faithful low-dimensional embeddings under strict privacy and communication constraints.

Anchors therefore play a central role in our framework, and their use is both practical and robust. Curated by a trusted server, they can be synthetic, anonymized, or drawn from public data, decoupled from private client records. This avoids leakage risks from client-generated anchors, especially in small or skewed regimes (Qiao et al., 2024) while providing stability, auditability, and adversarial robustness. Such strategies are already common in healthcare (Johnson et al., 2016; Bycroft et al., 2018), genomics (Regev et al., 2017; Litviňuková et al., 2020), finance (Awosika et al., 2024a), mobile/NLP applications (Hard et al., 2019; Li et al., 2019), and wireless sensor networks (Di Franco et al., 2017), illustrating their practical viability. Motivated by this, we treat anchors as core architectural components. SENSE leverages them, together with tools from distance matrix completion, network localization, and low-rank recovery, to provide formal privacy guarantees for reconstructing global structure from partial observations. It introduces the following key innovations:

- *Privacy and communication efficiency:* Distance estimation is decoupled from raw data, avoiding reliance on external mechanisms such as Homomorphic Encryption or Differential Privacy. Also, it requires only a single client–server interaction with no iterative training.
- Geometric and deployment flexibility: Supports both Euclidean and hyperbolic spaces and adapts to four observation regimes. As shown in Figure 1, these regimes dictate which entries of the distance matrix are observable. SENSE estimates/infers the missing inter-client similarity from this incomplete information while preserving privacy across all scenarios. In the *Pointwise* setting, each client contributes only a single non-anchor (NA), typical of edge/mobile devices, whereas in the *Multisite* setting, clients hold multiple NAs, such as patients in hospitals or customers in banks.
- Provable reliability: Provides formal privacy guarantees, complemented by empirical validation across diverse datasets and geometries.

Practical Impact. These properties make SENSE broadly applicable to privacy-sensitive, structurally diverse domains. Hospitals can jointly visualize patient data without violating HIPAA/GDPR (Sheller et al., 2019), banks can detect fraud patterns without exposing transac-

 tions (Awosika et al., 2024b), and even mobile/IoT devices with a single sample can contribute to global embeddings (Pape & Rannenberg, 2019; Baran, 1964). Genomic labs can embed single-cell transcriptomes into a shared hyperbolic space that preserves both cellular hierarchy and privacy (Agnihotry et al., 2022; Tasissa & Lai, 2019). Crucially, SENSE also supports dynamic participation: new clients or samples can be incorporated by estimating partial distances to existing entities, avoiding full re-computation while maintaining global coherence. Thus, SENSE is not only privacy-preserving and geometry-aware but also inherently scalable to dynamic federated ecosystems.

2 Background and Problem Formulation.

Neighbor Embedding (NE). Methods like t-SNE (van der Maaten & Hinton, 2008) and UMAP (Damrich & Hamprecht, 2021) embed high-dimensional data $\mathbf{X} = \{x_i\}_{i=1}^n \subset \mathbb{R}^{d_h}$ into a low-dimensional space $\mathbf{Y} = \{y_i\}_{i=1}^n \subset \mathbb{R}^{d_\ell}$ by preserving pairwise structure. These methods are distance-driven. They transform distances into similarities via kernels to preserve relational structure (see Appendix A.1, A.2). Let $\mathbf{D}_{ij}^{d_h} = \|x_i - x_j\|$ and $\mathbf{D}_{ij}^{d_\ell} = \|y_i - y_j\|$ denote distances in the high-and low-dimensional spaces respectively. These are mapped to similarities via kernel functions: $S_{ij}^{d_h} = f(\mathbf{D}_{ij}^{d_h})$, $S_{ij}^{d_\ell} = g(\mathbf{D}_{ij}^{d_\ell})$, where f and g are typically Gaussian, Laplacian, or Cauchy kernels. The general NE objective minimizes the divergence between the two similarity matrices:

$$\mathcal{L}(\mathbf{Y}) = \sum_{i,j} \mathcal{D}(S_{ij}^{d_h}, S_{ij}^{d_\ell}), \tag{1}$$

where \mathcal{D} is a divergence measure such as KL divergence or binary cross-entropy.

Contrastive Neighbor Embedding. CNE (Damrich et al., 2023) extends NE into the contrastive learning framework by training an encoder f_{θ} to map \mathbf{x}_i to $\mathbf{y}_i = f_{\theta}(\mathbf{x}_i)$ such that the neighborhood structure from a k-NN graph is preserved (Li et al., 2024). CNE uses a distance-aware contrastive loss (see Def A.3 in Appendix), framed as a binary similarity matching problem. Let $S^{d_h} \in \{0,1\}^{n \times n}$ denote ground-truth neighborhood indicators and S^{d_l} denote kernel-based similarities in the embedding space. The loss is a weighted binary cross-entropy:

$$\mathcal{L}(\mathbf{Y}) = -\sum_{i,j} \left[S_{ij}^{d_h} \log S_{ij}^{d_l} + b(1 - S_{ij}^{d_h}) \log(1 - S_{ij}^{d_l}) \right]. \tag{2}$$

where b > 0 balances the repulsion term; for more details on Eq. 2 see A.3.

Key Challenges in Decentralized Settings. (C1) CNE, like NE, relies on a full similarity matrix, which is unavailable in privacy-sensitive, decentralized settings. (C2) Conventional distributed learning captures only intra-client structure, omitting crucial inter-client neighbor information. (C3) Clients lack access to global data, leading to incorrect kNN graphs and biased negative sampling, as true neighbors may reside on other clients.

CO-SNE (for Hyperbolic Data). Hierarchical structures in social, biological, and knowledge graphs grow exponentially, making Euclidean embeddings unsuitable due to distortion of tree-like geometry. Hyperbolic space, with constant negative curvature, naturally models such growth and supports hierarchy-aware learning (Malik et al., 2025; Ganea et al., 2018) (see Appendix A.3.1). Standard methods like t-SNE assume Euclidean geometry and distort global structure when applied to hyperbolic data, collapsing depth and relative positioning. CO-SNE (Guo et al., 2022) extends t-SNE to hyperbolic geometry by using distance-aware kernels: $S_{ij}^{d_h} = f(d_{\mathbb{B}^n}(x_i, x_j))$, $S_{ij}^{d_l} = g(d_{\mathbb{B}^2}(y_i, y_j))$, where f is a hyperbolic normal kernel and g a heavy-tailed Cauchy kernel. A depth-regularization term aligns norms across spaces. The objective is:

$$\mathcal{L}(\mathbf{Y}) = \lambda_1 \cdot \mathcal{D}(S^{d_h}, S^{d_l}) + \lambda_2 \sum_i (\rho(x_i) - \rho(y_i))^2, \tag{3}$$

where $\rho(x) = ||x||$ and \mathcal{D} is typically KL divergence. For more details see Def A.4.

2.1 PROBLEM FORMULATION

We consider a decentralized system with M clients $\{\mathcal{C}_1,\ldots,\mathcal{C}_M\}$ coordinated by a central server owned by a private company, hospital, bank, or government agency. Each client \mathcal{C}_m holds a private dataset $\mathcal{D}_m = \{\mathbf{x}_i^m\}_{i=1}^{N_m} \subset \mathbb{R}^{d_h}$, which remains local and disjoint, i.e., $\mathcal{D}_m \cap \mathcal{D}_{m'} = \emptyset$ for $m \neq m'$. Let $N = \sum_{m=1}^M N_m$ be the total number of data points, indexed globally by $i \in [N]$. We consider two real-world configurations: A) SENSE-Pointwise, where each client holds a single sample $\mathbf{x}^m \in \mathbb{R}^{d_h}$,

and B) SENSE-Multisite, where each client holds a local dataset $\mathbf{X}^m = [\mathbf{x}_1^m, \dots, \mathbf{x}_{N_m}^m] \in \mathbb{R}^{N_m \times d_h}$. Let $\mathbf{D} \in \mathbb{R}^{N \times N}$ denote the full squared distance matrix. In Euclidean space, $\mathbf{D}_{ij} = \|\mathbf{x}_i - \mathbf{x}_j\|^2$; in hyperbolic space, it reflects squared distances in the Poincaré ball \mathbb{B}^{d_h} or Lorentz model \mathbb{H}^{d_h} (see Appendix A.3). Due to privacy constraints, only a subset of entries is observable. Let $\Omega \subseteq [N] \times [N]$ be the set of observed indices, and define the projection operator $\mathcal{P}_{\Omega} : \mathbb{R}^{N \times N} \to \mathbb{R}^{N \times N}$ as:

$$[\mathcal{P}_{\Omega}(\mathbf{D})]_{ij} = \begin{cases} \mathbf{D}_{ij}, & \text{if } (i,j) \in \Omega, \\ 0, & \text{otherwise.} \end{cases}$$
 (4)

Goal 1 Our goal is to reconstruct the full distance matrix from partial observations $\mathbf{D}_{\Omega} = \mathcal{P}_{\Omega}(\mathbf{D})$ via structured matrix completion. Rather than estimating distances directly, we infer latent embeddings $\hat{\mathbf{X}} \in \mathbb{R}^{N \times d_h}$ whose induced distances agree with the observed entries. Formally, we solve:

$$\widehat{\mathbf{X}}^{\star} = \arg\min_{\widehat{\mathbf{X}}} \left\| \mathcal{P}_{\Omega} \left(\mathcal{D}(\widehat{\mathbf{X}}) \right) - \mathbf{D}_{\Omega} \right\|_{F}^{2}, \tag{5}$$

and define the reconstructed distance matrix as $\widehat{\mathbf{D}} = \mathcal{D}(\widehat{\mathbf{X}}^*)$, which serves as an approximation of the true but unknown \mathbf{D} . Here $\mathcal{D}(\widehat{\mathbf{X}})$ denotes the induced pairwise distance matrix under the chosen geometry (Euclidean or hyperbolic). From $\widehat{\mathbf{D}}$, we then derive a global low-dimensional embedding $\mathbf{Y} = \{\mathbf{y}_i\}_{i=1}^N \subset \mathbb{R}^{d_\ell}$ with $d_\ell \ll d_h$, which preserves the neighborhood structure.

We use $\widehat{\mathbf{D}}$ to find the similarities, defined in Eq. 6 and optimized via divergence $\mathcal{D}(S^{d_h}, S^{d_\ell})$ (Eq. 1).

$$S_{ij}^{d_{h}} = \exp\left(-\frac{\widehat{\mathbf{D}}_{ij}}{2\sigma^{2}}\right), \quad S_{ij}^{d_{\ell}} = g(\|\mathbf{y}_{i} - \mathbf{y}_{j}\|^{2}), \tag{6}$$

For contrastive learning, we build binary similarities using k-nearest neighbors:

$$S_{ij}^{d_{h}} = \begin{cases} 1, & \text{if } j \in \text{kNN}(i; \widehat{\mathbf{D}}), \\ 0, & \text{otherwise,} \end{cases} \qquad S_{ij}^{d_{\ell}} = \phi(\mathbf{y}_{i}, \mathbf{y}_{j}) = \frac{1}{1 + \|\mathbf{y}_{i} - \mathbf{y}_{j}\|^{2}}, \tag{7}$$

and minimize the contrastive loss (Eq. 2). For hierarchical data, we apply CO-SNE, treating $\widehat{\mathbf{D}}$ as squared hyperbolic distances in the Poincaré model to compute similarities (Eq. 16 in Appendix). The embedding $\mathbf{Y} \subset \mathbb{B}^{d_\ell}$ is optimized using the CO-SNE loss (Eq. 3).

3 PROPOSED FRAMEWORK: SENSE

As described in Section 2.1, we consider two decentralized settings: SENSE-Pointwise and SENSE-Multisite. In both, each client holds private non-anchor (NA) data and accesses a shared anchor set $\mathcal{A} = \{a_1, \ldots, a_K\}$ with feature matrix $\mathbf{X}_A = [\mathbf{p}_1, \ldots, \mathbf{p}_K]^\top \in \mathbb{R}^{K \times d_h}$. Anchors, broadcast by the server, may be global or client-specific (see Appendix A.8). Let $\mathcal{X} = \{x_1, \ldots, x_N\}$ be the set of all private NA points (raw features), where $N = \sum_{m=1}^M N_m$. Each client computes squared distances between its NAs and accessible anchors:

$$\mathbf{d}_{i}^{m} = [\|x_{i}^{m} - \mathbf{p}_{1}\|^{2}, \dots, \|x_{i}^{m} - \mathbf{p}_{K}\|^{2}],$$

and transmits these to the server, masking unshared local anchors. In *Pointwise*, each client contributes one NA-anchor vector, in *Multisite*, intra-client NA–NA distances may also be known. The global incomplete squared distance matrix $\mathbf{D} \in \mathbb{R}^{(K+N)\times (K+N)}$ is partitioned as:

$$\mathbf{D} = \begin{bmatrix} E & F \\ F^{\top} & G \end{bmatrix},\tag{8}$$

where E is anchor–anchor, F is anchor–NA, and G is NA–NA. The observed subset is indexed by $\Omega\subseteq [K+N]^2$, based on anchor visibility and client configuration. We consider four configurations: Pointwise-Full, Pointwise-Partial, Multisite-Full, and Multisite-Partial which differ in the extent of observed entries in F (anchor–NA) and G (NA–NA). These define distinct visibility patterns in Ω , summarized in Appendix Table 6 and illustrated in Figure 1, and determine which distances are available for structured matrix completion. To reconstruct the unobserved blocks of \mathbf{D} (notably G) and obtain the Pointsite Pointsite

Remark 1 In practice, F may be only partially or fully visible due to bandwidth, privacy, or data limitations. SENSE is designed to operate under such conditions.

3.1 SENSE VIA ANCHORED-MDS

Classical MDS embeds N points by minimizing stress over a fully observed distance matrix $\mathbf{D} \in \mathbb{R}^{N \times N}$. The embedding $\mathbf{X} \in \mathbb{R}^{N \times d_h}$ minimizes: $\sigma(\mathbf{X}) = \sum_{i < j} (\|x_i - x_j\| - \delta_{ij})^2$, where δ_{ij} is the input Euclidean distance between points i and j. SMACOF solves this using a majorization-based surrogate (De Leeuw, 2005) (details in Appendix A.5), $\tau(\mathbf{X}, \mathbf{Z}) = C + \operatorname{tr}(\mathbf{X}^{\top}\mathbf{V}\mathbf{X}) - 2\operatorname{tr}(\mathbf{X}^{\top}\mathbf{B}(\mathbf{Z})\mathbf{Z})$, with the iterative update:

$$\mathbf{X}^{(k)} = \mathbf{V}^{\dagger} \mathbf{B} (\mathbf{X}^{(k-1)}) \mathbf{X}^{(k-1)}. \tag{9}$$

In SENSE, we do not observe the full matrix \mathbf{D} (in Eq. 8), instead, we only access the observed entries $\mathbf{D}_{\Omega} = \mathcal{P}_{\Omega}(\mathbf{D})$, which contain distances on a subset of pairs. Let the embedding be $\mathbf{X} = [\mathbf{X}_A \ \mathbf{X}_{NA}]^{\top}$, where \mathbf{X}_A and \mathbf{X}_{NA} are anchor and NA embeddings, respectively. Stress is minimized over observed entries only: $\sigma(\mathbf{X}) = \|\mathcal{P}_{\Omega}(\mathcal{D}(\mathbf{X}) - \mathbf{D})\|_F^2$, where \mathcal{P}_{Ω} projects onto observed indices Ω , and $\mathcal{D}(\mathbf{X})$ computes pairwise distances. The SMACOF updates are restricted to Ω , with:

$$V_{ij} = \begin{cases} |\{j: (i,j) \in \Omega\}|, & i = j \\ -1, & (i,j) \in \Omega, \ i \neq j \\ 0, & \text{otherwise} \end{cases}, \quad B_{ij}(\mathbf{X}) = \begin{cases} -\frac{\delta_{ij}}{\|x_i - x_j\|}, & (i,j) \in \Omega, \ i \neq j \\ -\sum\limits_{k \neq i, \ (i,k) \in \Omega} B_{ik}, & i = j \\ 0, & \text{otherwise} \end{cases}$$

We partition V and B as defined in Eq. 10, where $V_{AA}, B_{AA} \in \mathbb{R}^{K \times K}, V_{AN}, B_{AN} \in \mathbb{R}^{K \times N}$, and $V_{NN}, B_{NN} \in \mathbb{R}^{N \times N}$:

$$\mathbf{V} = \begin{bmatrix} \mathbf{V}_{AA} & \mathbf{V}_{AN} \\ \mathbf{V}_{AN}^{\top} & \mathbf{V}_{NN} \end{bmatrix}, \quad \mathbf{B} = \begin{bmatrix} \mathbf{B}_{AA} & \mathbf{B}_{AN} \\ \mathbf{B}_{AN}^{\top} & \mathbf{B}_{NN} \end{bmatrix}$$
(10)

The update rule for NA embeddings becomes:

$$\mathbf{X}_{NA}^{(k)} = \mathbf{V}_{NN}^{\dagger} \left(\mathbf{B}_{NN} \mathbf{X}_{NA}^{(k-1)} + \mathbf{B}_{AN}^{\top} \mathcal{P}_{\Omega}(\mathbf{X}_A) - \mathbf{V}_{AN}^{\top} \mathcal{P}_{\Omega}(\mathbf{X}_A) \right). \tag{11}$$

This projection-aware update ensures X_{NA} uses only observed/available distances. The projection operator \mathcal{P}_{Ω} acts as a binary mask over observed entries. While V and B are derived from Ω , we apply \mathcal{P}_{Ω} to X_A in Eq. 11 to retain only anchors with observed anchor–NA distances. This avoids leakage from inaccessible anchors and ensures privacy-compliant updates (pseudocode in Appendix A.7). Furthermore, to preserve privacy, the number of shared anchors K must be limited. Theorems 3.1, 3.2 (Euclidean) and Lemma 1 (hyperbolic) characterize how K relates to embedding dimension d_h across SENSE configurations, establishing privacy conditions for faithful reconstruction.

Theorem 3.1 Let $\mathcal{X} = \{\mathbf{x}_1, \dots, \mathbf{x}_N\} \subset \mathbb{R}^{d_h}$ be the set of NA data points, and let $\mathcal{A} = \{\mathbf{a}_1, \dots, \mathbf{a}_K\} \subset \mathbb{R}^{d_h}$ be the set of K anchor points. Suppose we observe the pairwise Euclidean distances $\{\|\mathbf{x}_i - \mathbf{a}_j\|\}_{i \in [N], j \in [K]}$ between each NA and all anchors. If the number of anchors satisfies $K < d_h$, then the original NA features $\{\mathbf{x}_i\}_{i=1}^N$ cannot be exactly reconstructed from these distances, guaranteeing the privacy of the individual client data. *Proof.* Deferred in Appendix, check A.1.

While Theorem 3.1 ensures privacy, the reconstructed embeddings (Eq. 11) must also remain useful. We capture this through *reconstruction fidelity*, defined as preserving neighborhood structure rather than exact features. In SENSE, such fidelity is guaranteed by well-established results from MDS distance-based recovery (Drineas et al., 2006; Zhang et al., 2019; Lichtenberg & Tasissa, 2024a). These solvers are known to produce embeddings consistent up to Euclidean isometries (translation, rotation, and scaling) (Mardia & Riley, 2021; Khan et al., 2009). These invariances ensure that geometric relationships are preserved for downstream tasks, while exact feature values remain unrecoverable, achieving precisely the balance required in privacy-sensitive settings.

SENSE supports multiple configurations, which critically influence embedding fidelity and privacy. Theorem 3.2 formalizes privacy guarantees when only partial anchor–NA distances (block F) are available, covering both *pointwise* and *multisite* regimes. 1) SENSE-Pointwise: Each client $j \in [N]$ holds a single private point $\boldsymbol{x}_j \in \mathbb{R}^{d_h}$ and accesses a subset of anchors indexed by $\mathcal{I}_j \subseteq [K]$. The corresponding anchor set is $\mathcal{A}_j = \{\boldsymbol{a}_i\}_{i \in \mathcal{I}_j}$, comprising: (i) global anchors $\mathcal{A}_G = \{\boldsymbol{a}_1, \dots, \boldsymbol{a}_{M_G}\}$, shared across all clients, and (ii) local anchors $\mathcal{A}_L^{(j)}$, unique to client j. The total of anchors observed is $r_j = |\mathcal{I}_j| = M_G + M_L^{(j)}$. 2) SENSE-Multisite: Each client $m \in [M]$ holds a local dataset $\mathcal{X}^{(m)} = \{\boldsymbol{x}_{m,1}, \dots, \boldsymbol{x}_{m,n_m}\} \subset \mathbb{R}^{d_h}$, where $N = \sum_{m=1}^M n_m$. Each point $\boldsymbol{x}_{m,i}$ observes distances

to (i) a shared global anchor set A_G , and (ii) a local anchor set $A_L^{(m)}$ exclusive to client m. Let $\mathcal{I}_{m,i} = \mathcal{I}_G \cup \mathcal{I}_L^{(m)}$ be index set of accessible anchors, with $r_{m,i} = |\mathcal{I}_{m,i}|$ denoting number observed.

Theorem 3.2 Let $\mathcal{X} = \{x_1, \dots, x_N\} \subset \mathbb{R}^{d_h}$ be the set of all non-anchor (NA) points across all clients, where each x_i computes squared distances only to a subset of accessible anchors $A_i = \{a_j\}_{j \in \mathcal{I}_i}$, with $|\mathcal{I}_i| = r_i$. If $r_i < d_h$ for all $i \in [N]$, then exact recovery of each x_i is impossible. The inverse map from anchor distances to features is non-unique, preserving privacy under both pointwise and multisite configurations.

Proof. Deferred in Appendix, check A.2.

Lemma 1 Let $\{x_1, \ldots, x_{K+N}\} \subset \mathbb{H}^{d_h}$ be K anchors and N NA points in hyperbolic space with curvature $-\kappa$. Suppose only blocks E and F of distance matrix \mathbf{D} are observed. If $K < d_h$, the NA coordinates cannot be exactly recovered up to isometry in \mathbb{H}^{d_h} , ensuring the privacy of the client data in SENSE. This follows from the contrapositive of the L-HYDRA theorem (Keller-Ressel & Nargang, 2022), which guarantees exact recovery only when $K \ge d_h$ and anchors span a full subspace.

In SENSE, we deliberately restrict anchors to $K < d_h$ rather than $K \le d_h$. Fewer anchors enlarge the feasible solution space, introducing geometric ambiguity (Wei et al., 2015; Liberti et al., 2014) that strengthens privacy while still preserving neighborhood structure (Fig. 3). This design holds in both Euclidean and hyperbolic spaces, making it a general, geometry-agnostic choice. A detailed theoretical discussion and supporting examples are provided in Appendix A.10.

4 EXPERIMENTS

In this section, we first outline the experimental setup, followed by an evaluation of SENSE across diverse datasets and deployment settings.

4.1 EXPERIMENTAL SETUP

Datasets. We evaluate SENSE on 14 public datasets widely used in DR and representation learning (Fu et al., 2024). These include three benchmarks: MNIST (Deng, 2012), Fashion-MNIST (Xiao et al., 2017), and CIFAR-10 (Giuste & Vizcarra, 2020); seven MedMNIST datasets (Yang et al., 2023): DermaMNIST, PneumoniaMNIST, RetinaMNIST, BreastMNIST, BloodMNIST, OrganCMNIST, OrganSMNIST; and the German Credit dataset (Hofmann, 1994). For hyperbolic, we use three graph datasets: Airport (Malik et al., 2025), Amazon (Yang & Leskovec, 2012), and DBLP (Kataria et al., 2024). Detailed dataset stats and system specifications are in Appendix Table 7 and A.13.

Baselines. We compare SENSE against centralized (Van) baselines: t-SNE (van der Maaten & Hinton, 2008), UMAP (McInnes et al., 2020), PHATE (Moon et al., 2019), and CNE (Damrich et al., 2023) (with $s \in \{0, 0.5, 1\}$). These assume full raw data access at a central server and serve as upper bounds for evaluating SENSE's privacy-preserving performance.

Implementation Details. SENSE has two stages: matrix completion and global embedding. In the first stage, data is partitioned across M clients. In Pointwise, each client holds one NA point, sampled randomly. In Multisite, clients hold multiple NA points under IID or non-IID splits (balanced/unbalanced). A subset of 10% of the total data points is designated as anchors. In Full settings, all anchors are global, and in Partial, anchors are split into global and client-specific local sets. The total of anchors (global + local) is fixed at $d_h - 1$, where d_h is the original feature dimension. In the embedding stage, we use the completed distance matrix to generate privacy-preserving embeddings using multiple neighbor embedding methods. For Euclidean geometry, we use the official implementations of t-SNE (van der Maaten & Hinton, 2008), UMAP (McInnes et al., 2020), and PHATE (via its standard Python library). For CNE, we adopt the implementation from (Damrich et al., 2023), where the parameter s controls the attraction-repulsion tradeoff: s=0 mimics t-SNE, s=1 aligns with UMAP, and intermediate values interpolate between them. CNE operates within a contrastive learning framework using negative sampling. For hyperbolic embeddings, we use the CO-SNE implementation from (Guo et al., 2022).

Remark 2 The 10% anchor sharing in the multisite setting is used only for empirical evaluation. These anchors are not private; they act as public or semi-public landmarks, akin to those in GPS (Shang & Ruml, 2004) or radar systems (lannucci et al., 2020). This is standard in localization literature (Di Franco et al., 2017; Khan et al., 2009), where landmarks aid positioning but are not privacy-sensitive (Koledoye et al., 2017). Our privacy definition protects only the high-dimensional features of NA points. Anchors are fixed, visible, and either synthetic, public, or explicitly consented. Not part of any client's private data. For details on anchor generation, see Appendix A.8.

Table 1: Full vs. Partial comparison in MULTISITE under non-IID (unbalanced) splits. Evaluation spans centralized and privacy-preserving SENSE variants across different embedding quality metrics.

Data	Metric	t-S	NE	UM	IAP	PH	ATE	CNE	(s=0)	CNE(s=0.5)	CNE	(s=1)
		VAN.	SENSE	VAN.	SENSE	VAN.	SENSE	VAN.	SENSE	VAN.	SENSE	VAN.	SENSE
					— Multis	ite-Partia	l Setting -	_					
	Trust.	0.9890	0.9898	0.9553	0.9552	0.8741	0.8763	0.9517	0.9521	0.9524	0.9538	0.9455	0.9476
MNIST	Cont.	0.9575	0.9639	0.9774	0.9771	0.9811	0.9804	0.9806	0.9797	0.9799	0.9787	0.9799	0.9787
MINIST	Stead.	0.7719	0.7861	0.7639	0.7635	0.6628	0.6746	0.7840	0.7790	0.7752	0.7768	0.7634	0.7658
	Cohes.	0.8189	0.8458	0.8865	0.8853	0.8668	0.8877	0.9229	0.9112	0.9107	0.9196	0.9158	0.9087
	Trust.	0.9902	0.9914	0.9140	0.9148	0.9579	0.9557	0.9765	0.9752	0.9784	0.9769	0.9765	0.9731
fashionMNIST	Cont.	0.9608	0.9590	0.9812	0.9818	0.9910	0.9906	0.9915	0.9913	0.9905	0.9903	0.9900	0.9901
Tasinonivityi3 I	Stead.	0.8415	0.8643	0.7570	0.7622	0.7836	0.7891	0.8632	0.8638	0.8643	0.8660	0.8493	0.8513
	Cohes.	0.6496	0.6559	0.6748	0.7069	0.7051	0.7115	0.7680	0.7669	0.7637	0.7508	0.7792	0.7666
— Multisite-Full Setting —													
	Trust.	0.9890	0.9852	0.9553	0.9570	0.8741	0.8780	0.9517	0.9516	0.9524	0.9542	0.9455	0.9452
MNIST	Cont.	0.9575	0.9518	0.9774	0.9754	0.9811	0.9797	0.9806	0.9772	0.9799	0.9763	0.9799	0.9761
MINIST	Stead.	0.7719	0.7953	0.7639	0.7726	0.6628	0.6688	0.7840	0.7808	0.7752	0.7828	0.7634	0.7690
	Cohes.	0.8189	0.8328	0.8865	0.8665	0.8668	0.8818	0.9229	0.9047	0.9107	0.8926	0.9158	0.9106
	Trust.	0.9902	0.9895	0.9140	0.9076	0.9579	0.9555	0.9765	0.9752	0.9784	0.9769	0.9765	0.9725
fashionMNIST	Cont.	0.9608	0.9731	0.9812	0.9797	0.9910	0.9902	0.9915	0.9906	0.9905	0.9895	0.9900	0.9891
Tasinonivityi3 I	Stead.	0.8415	0.8604	0.7570	0.7530	0.7836	0.7981	0.8632	0.8608	0.8643	0.8649	0.8493	0.8538
	Cohes.	0.6496	0.6936	0.6748	0.7019	0.7051	0.7039	0.7680	0.7503	0.7637	0.7591	0.7792	0.7695
					— Point	wise-Full	Setting —	-					
	Trust.	0.9661	0.9679	0.9484	0.9467	0.8457	0.8469	0.9218	0.9166	0.9164	0.9138	0.9137	0.9151
	Cont.	0.9418	0.9410	0.9376	0.9396	0.9546	0.9538	0.9434	0.9422	0.9428	0.9417	0.9409	0.9403
MNIST	Stead.	0.8083	0.8113	0.7878	0.7763	0.6953	0.6958	0.8024	0.8003	0.8041	0.7996	0.8025	0.7914
I CIVIIVI	Cohes.	0.7904	0.7998	0.7855	0.7819	0.7912	0.7843	0.7988	0.7982	0.8034	0.7894	0.7931	0.7919
	Trust.	0.9647	0.9681	0.9441	0.9434	0.8407	0.8375	0.9283	0.9264	0.9255	0.9245	0.9256	0.9196
	Cont.	0.9430	0.9454	0.9386	0.9373	0.9542	0.9528	0.9464	0.9460	0.9456	0.9440	0.9451	0.9429
fashionMNIST	Stead.	0.8118	0.8103	0.7797	0.7779	0.6923	0.6931	0.8087	0.8049	0.8085	0.8003	0.8082	0.8150
1 GINIIVIIIVIIIO	Cohes.	0.7570	0.7882	0.7685	0.7670	0.7564	0.7599	0.7876	0.7786	0.7843	0.7788	0.7838	0.7710

Data Partitioning. To simulate realistic distributed settings, we evaluate SENSE under both IID and non-IID distributions using Dirichlet-based partitioning. For each class c, client-wise proportions are drawn from $q_c \sim \text{Dir}(\alpha)$, where lower α yields greater heterogeneity and class imbalance (Wang et al., 2020; Zhao et al., 2018). We set $\alpha = 0.5$ in all experiments. Three partitioning schemes are used: *IID* (uniform class mix), non-IID balanced (varying class distributions, equal client sizes), and non-IID unbalanced (both class and size vary).

Evaluation Metrics. We assess SENSE using both reconstruction and embedding quality metrics. For fidelity, we compute *Relative Distance Error (DE)* and *F-score (FS)* between the reconstructed distance matrix (NA-NA) \hat{G} and ground truth G_{true} : DE = $\frac{\|\hat{G} - G_{\text{true}}\|_F}{\|G_{\text{true}}\|_F}$, and FS = $\frac{2 \text{ tp}}{2 \text{ tp} + \text{fp} + \text{fn}}$, where tp, fp, and fn are true, false positive, and false negative neighbors respectively (Egilmez et al., 2017). To evaluate 2D embeddings, we compute *Trustworthiness* and *Continuity* (Venna & Kaski, 2005), which measure neighborhood agreement between original and embedded spaces. We also report *Steadiness* and *Cohesiveness* (Jeon et al., 2021) to assess global structural reliability: steadiness detects false groupings and cohesiveness quantifies how well true input clusters are preserved.

4.2 RESULT ANALYSIS.

We comprehensively evaluate SENSE across: 1) Standard image datasets (MNIST, FashionMNIST, CIFAR-10): These are evaluated under Pointwise-Full, Multisite-Full, and Multisite-Partial with non-IID unbalanced splits. As shown in Table 1 and in Appendix 10, SENSE closely matches centralized baselines across Cont., Trust., Stead., and Cohes. Notably, the Partial configuration performs comparably to Full, indicating that accurate reconstruction of the global distance matrix is possible even with partial anchor–NA observations. Table 9 further confirms high F-score and low distance error, validating strong neighborhood preservation under strict privacy constraints.

2) MedMNIST datasets: These are evaluated across unbalanced non-IID, balanced non-IID, and IID splits. SENSE consistently matches centralized performance (Tables 3,12,11), even under high heterogeneity. Table 8 in Appendix, further shows low DE and high FS, confirming strong structural and similarity preservation. 3) Hyperbolic datasets (Airport, Amazon, DBLP): For these datasets, the results in Table 2 highlight SENSE's geometry-aware design, achieving high FS and very low DE in non-Euclidean

Table 2: FS and DE for hyperbolic datasets in POINTWISE setting.

Dataset	FS	DE
AIRPORT AMAZON DBLP	0.9992 0.9945 0.9929	0.000067 0.00052 0.00073

spaces. This confirms its adaptability across geometric regimes. Overall, SENSE effectively ensures:

 Neighbor preservation: High continuity and trustworthiness show SENSE keeps similar points close in the embedding, preserving semantics across clients.

Table 3: Performance of centralized (Van.) and SENSE variants under non-IID unbalanced splits.

Data	Metric	t-S	NE	UN	IAP	PH	ATE	CNI	E(s=0)	CNE(s=0.5)	CNE	(s=1)
		VAN.	SENSE	VAN.	SENSE	VAN.	SENSE	VAN.	SENSE	VAN.	SENSE	VAN.	SENSE
	Trust.	0.9723	0.9712	0.7699	0.7673	0.8570	0.8590	0.9027	0.9008	0.8976	0.8952	0.8832	0.8806
	Cont.	0.9418	0.9383	0.9140	0.9154	0.9624	0.9608	0.9594	0.9591	0.9590	0.9583	0.9606	0.9599
PneumoniaMNIST	Stead.	0.7868	0.7932	0.6258	0.6168	0.7247	0.7204	0.7552	0.7591	0.7496	0.7461	0.7283	0.7341
PheumomawiNiSi	Cohes.	0.6991	0.6591	0.6318	0.6250	0.6953	0.6957	0.6983	0.7085	0.7052	0.7142	0.7015	0.7065
	Trust.	0.9633	0.9609	0.8674	0.8632	0.8493	0.8513	0.8841	0.8816	0.8814	0.8795	0.8737	0.8715
	Cont.	0.9256	0.9375	0.9411	0.9401	0.9435	0.9428	0.9555	0.9552	0.9558	0.9556	0.9555	0.9552
BloodMNIST	Stead.	0.7498	0.7480	0.6889	0.6874	0.6781	0.6851	0.7172	0.7323	0.7186	0.7216	0.7100	0.7132
Dioodiviivisi	Cohes.	0.7242	0.7178	0.7253	0.7253	0.7456	0.7448	0.7462	0.7440	0.7384	0.7540	0.7533	0.7379
	Trust.	0.9379	0.9378	0.7817	0.7998	0.8921	0.8884	0.9133	0.9117	0.9124	0.9113	0.9108	0.9108
	Cont.	0.9508	0.9481	0.8140	0.8247	0.9616	0.9563	0.9519	0.9515	0.9516	0.9513	0.9510	0.9509
BreastMNIST	Stead.	0.8417	0.8329	0.5605	0.5550	0.8037	0.8149	0.8438	0.8480	0.8491	0.8495	0.8490	0.8398
Dicastivityisi	Cohes.	0.6091	0.6137	0.4095	0.4112	0.5668	0.5570	0.5777	0.5695	0.5807	0.5689	0.5675	0.5585
	Trust.	0.9757	0.9770	0.7496	0.7466	0.8737	0.8728	0.9130	0.9121	0.9119	0.9116	0.9020	0.9021
	Cont.	0.9461	0.9572	0.9127	0.9122	0.9736	0.9730	0.9709	0.9713	0.9706	0.9707	0.9716	0.9715
DermaMNIST	Stead.	0.7977	0.7979	0.5945	0.5936	0.7308	0.7319	0.7739	0.7689	0.7682	0.7686	0.7578	0.7553
Defination	Cohes.	0.7147	0.7111	0.5586	0.5459	0.7127	0.7108	0.7268	0.7321	0.7385	0.7502	0.7438	0.7383
	Trust.	0.9797	0.9736	0.8793	0.8636	0.9161	0.9050	0.9486	0.9357	0.9475	0.9348	0.9451	0.9336
	Cont.	0.9496	0.9669	0.9273	0.9244	0.9738	0.9734	0.9720	0.9714	0.9707	0.9701	0.9678	0.9680
RetinaMNIST	Stead.	0.8442	0.8498	0.6307	0.5923	0.7559	0.7636	0.8267	0.8176	0.8196	0.8138	0.8158	0.8040
Remaining	Cohes.	0.6734	0.7281	0.5832	0.5828	0.6957	0.6991	0.7100	0.7137	0.7089	0.6982	0.6883	0.6990
	Trust.	0.9621	0.9387	0.8887	0.8867	0.8850	0.8871	0.9134	0.9041	0.9159	0.9056	0.9019	0.8907
	Cont.	0.9207	0.9170	0.9268	0.9247	0.9691	0.9699	0.9733	0.9693	0.9729	0.9685	0.9737	0.9696
OrganCMNIST	Stead.	0.7011	0.7855	0.7527	0.7718	0.7935	0.8093	0.8666	0.8755	0.8733	0.8722	0.8597	0.8607
Organiciviivisi	Cohes.	0.4685	0.5037	0.3322	0.3373	0.5431	0.5444	0.4653	0.5096	0.5681	0.5233	0.5745	0.5375
•	Trust.	0.9552	0.9357	0.8741	0.8625	0.8792	0.8821	0.9114	0.9028	0.9126	0.9040	0.8993	0.8912
	Cont.	0.9214	0.9169	0.9246	0.9213	0.9684	0.9700	0.9738	0.9682	0.9731	0.9675	0.9736	0.9683
OrganSMNIST	Stead.	0.6765	0.7311	0.7222	0.7485	0.7809	0.7995	0.8609	0.8659	0.8664	0.8708	0.8561	0.8582
Organisiviivisi	Cohes.	0.4951	0.4814	0.3603	0.3211	0.5198	0.5343	0.4704	0.44009	0.5192	0.4833	0.5155	0.5033
	Trust.	0.9745	0.9543	0.9514	0.9294	0.8555	0.8394	0.9337	0.9124	0.9380	0.9072	0.9336	0.9092
	Cont.	0.9583	0.9424	0.9604	0.9410	0.9481	0.9255	0.9571	0.9438	0.9576	0.9438	0.9571	0.9440
german-credit	Stead.	0.8576	0.8248	0.8313	0.7933	0.7483	0.7061	0.8398	0.7921	0.8479	0.7855	0.8436	0.7906
german-creun	Cohes.	0.6774	0.6755	0.6638	0.6568	0.6893	0.6745	0.6446	0.6551	0.6575	0.6481	0.6513	0.6676

- Similarity recovery: Despite no raw data access, SENSE accurately approximates pairwise distances evidenced by low DE and high FS.
- Cluster structure: Comparable steadiness and cohesiveness confirm that SENSE maintains cluster alignment without fragmentation.

Visualization. Figure 2 shows global embeddings learned by SENSE on MNIST in the MULTISITE setting with 25,000 NA samples across 10 clients in an unbalanced non-IID split. Using only 783 anchors (d_h-1) , SENSE constructs high-quality embeddings without accessing or sharing raw features. Embeddings from t-SNE, UMAP, PHATE, and CNE cleanly separate semantic groups, preserving local neighborhoods and global cluster topology. By estimating inter-client similarities, SENSE enables meaningful inter-client positive/negative contrastive pairs. This highlights its ability to learn structure-preserving, privacy-compliant embeddings in decentralized, heterogeneous settings. Additional visualizations are in the Appendix A.14.

4.3 ABLATION STUDY.

To validate Theorems 3.1, 3.2, and Lemma 1, we perform an ablation study by varying anchor count from $d_h - \epsilon$ to $d_h + \epsilon$. We evaluate SENSE using five normalized metrics, plotted in Figure 3: (i) Cosine Similarity (Nguyen & Bai, 2010) between ground-truth X'_{NA} and reconstructed latent embeddings \widehat{X}_{NA} ; (ii) Distance Error and (iii) F-score (Sec. 4.1); (iv) Pearson Correlation (ρ) (Sedgwick, 2012) over NA-NA distances; and (v) Frobenius Norm Error (X_{frob}) (Kannan, 1989), capturing reconstruction loss (full definitions in Appendix A.15). Key observations from the study:

- Effective with few anchors: Even with anchor count well below d_h (e.g., $d_h 100$), SENSE achieves high F-score, low distance error, and strong cosine similarity, showing robust neighborhood preservation in resource-constrained settings.
- Privacy-compliant reconstruction: As anchors approach d_h , cosine and Pearson scores improve. Beyond $d_h + 1$, near-zero Frobenius error indicates possible exact recovery highlighting the need to limit anchor count to preserve privacy.
- Structural consistency: Pearson correlation rises with anchor count, saturating near 1.0 at $d_h + 1$, with corresponding drops in Frobenius error confirming theoretical bounds for exact recovery.
- Metric alignment with theoretical thresholds: Across datasets, all metrics converge near d_h , with diminishing gains beyond matching theoretical thresholds.

These results validate that SENSE achieves high-fidelity, privacy-compliant reconstruction with minimal anchors, making it scalable and effective in decentralized settings with limited observability.

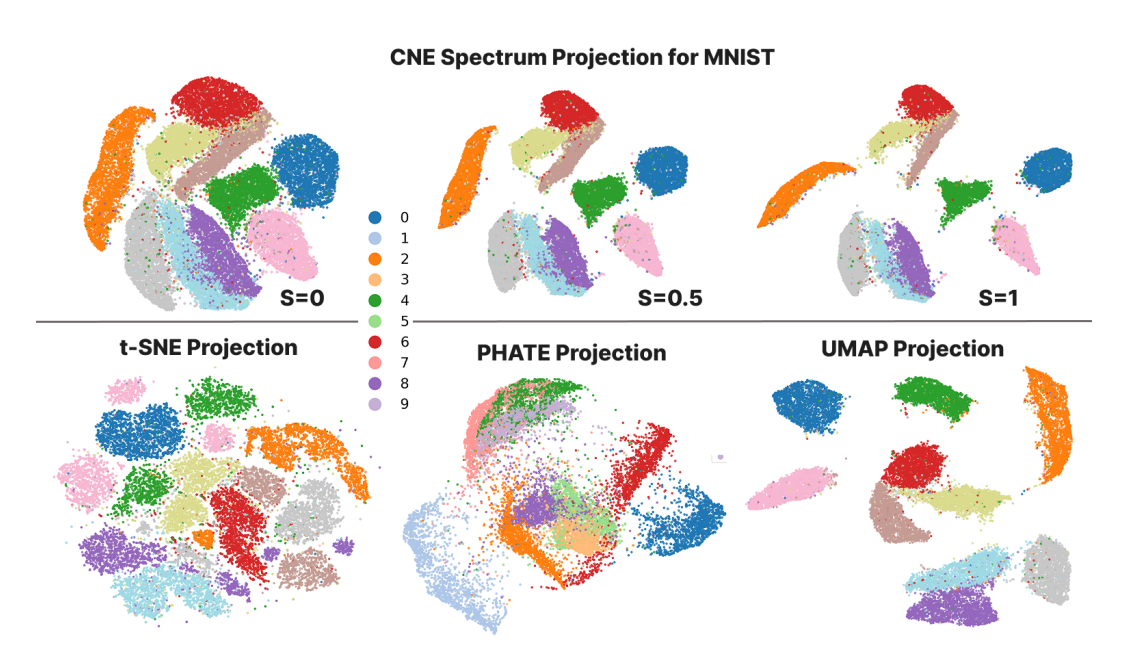


Figure 2: Global embeddings of MNIST under the MULTISITE setting. **Top:** CNE spectrum with SENSE. **Bottom:** t-SNE, PHATE, and UMAP embeddings generated via SENSE without any raw feature sharing. All embeddings preserve global structure while ensuring privacy.

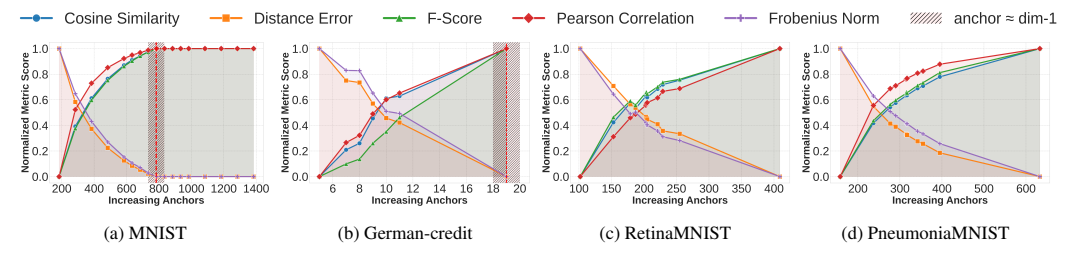


Figure 3: Impact of anchor count on normalized metric scores under non-IID unbalanced distributions. The red vertical line denotes the theoretical privacy threshold at d_h-1 (783 for MNIST, 19 for German Credit), beyond which exact recovery may be possible. For Retina and Pneumonia, this threshold lies outside the x-axis range, resulting in monotonic performance gains. Trends confirm trade-offs between reconstruction fidelity and privacy risk as anchor count increases.

4.4 DISCUSSION.

Due to space constraints, we provide the extended discussion of SENSE and additional empirical results in Appendix A.16. It addresses four key aspects: (i) how SENSE adapts to dynamic evolving distributed environments via out-of-sample embedding; (ii) scalability and runtime on large-scale datasets such as Tiny ImageNet (Le & Yang, 2015) and SVHN (Netzer et al., 2011) (Table 13), with a detailed breakdown of pipeline stages and complexity analysis in Table 14; (iii) a curated privacy example showing that embeddings preserve structural relationships while preventing recovery of sensitive attributes (Table 15); and (iv) why SENSE avoids noise-based privacy (Table 16 and 17), since injected noise quickly degrades embedding quality, whereas geometric underdetermination preserves both fidelity and privacy.

5 CONCLUSION

We proposed SENSE, a geometry-aware framework for decentralized representation learning that reconstructs global geometry from sparse anchor-based distances, enabling projections without raw data exchange. By combining structured matrix completion with classical DR methods, SENSE supports both Euclidean and hyperbolic spaces and adapts to multiple deployment settings. Experiments show that SENSE is effective even with few anchors, achieving strong neighborhood and cluster preservation while matching centralized baselines under strict privacy and communication constraints. These results highlight SENSE as a scalable, privacy-preserving solution for collaborative representation learning in heterogeneous, non-IID environments.

REFERENCES

- Martin Abadi, Andy Chu, Ian Goodfellow, H. Brendan McMahan, Ilya Mironov, Kunal Talwar, and Li Zhang. Deep learning with differential privacy. In *Proceedings of the 2016 ACM SIGSAC Conference on Computer and Communications Security*, CCS'16, pp. 308–318. ACM, October 2016. doi: 10.1145/2976749.2978318. URL http://dx.doi.org/10.1145/2976749.2978318.
- Shikha Agnihotry, Rajesh Kumar Pathak, Dev Bukhsh Singh, Apoorv Tiwari, and Imran Hussain. Protein structure prediction. In *Bioinformatics*, pp. 177–188. Elsevier, 2022.
- E. Alpaydin and C. Kaynak. Optical Recognition of Handwritten Digits. UCI Machine Learning Repository, 1998. DOI: https://doi.org/10.24432/C50P49.
- Tomisin Awosika, Raj Shukla, and Bernardi Pranggono. Transparency and privacy: The role of explainable ai and federated learning in financial fraud detection. *IEEE Access*, PP:1–1, 01 2024a. doi: 10.1109/ACCESS.2024.3394528.
- Tomisin Awosika, Raj Mani Shukla, and Bernardi Pranggono. Transparency and privacy: the role of explainable ai and federated learning in financial fraud detection. *IEEE Access*, 2024b.
- Paul Baran. On distributed communications networks. *IEEE transactions on Communications Systems*, 12(1):1–9, 1964.
- Yoshua Bengio, Jean-françcois Paiement, Pascal Vincent, Olivier Delalleau, Nicolas Roux, and Marie Ouimet. Out-of-sample extensions for lle, isomap, mds, eigenmaps, and spectral clustering. In S. Thrun, L. Saul, and B. Schölkopf (eds.), *Advances in Neural Information Processing Systems*, volume 16. MIT Press, 2003. URL https://proceedings.neurips.cc/paper_files/paper/2003/file/cf05968255451bdefe3c5bc64d550517-Paper.pdf.
- B Betti, M Crespi, and F Sanso. A geometric illustration of ambiguity resolution in gps theory and a bayesian approach. *Manuscripta geodaetica*, 18(5):317–330, 1993.
- Pratik Biswas and Yinyu Ye. Semidefinite programming for ad hoc wireless sensor network localization. In *Proceedings of the 3rd international symposium on Information processing in sensor networks*, pp. 46–54, 2004.
- Prosenjit Bose, Jean-Lou De Carufel, Alina Shaikhet, and Michiel Smid. Art gallery localization. *arXiv preprint arXiv:1706.06938*, 2017.
- Clare Bycroft, Colin Freeman, Desislava Petkova, Gavin Band, Lloyd T. Elliott, Kevin Sharp, Allan Motyer, Damjan Vukcevic, Olivier Delaneau, Jared O'Connell, Adrian Cortes, Samantha Welsh, Alan Young, Mark Effingham, Gil McVean, Stephen Leslie, Naomi Allen, Peter Donnelly, and Jonathan Marchini. The uk biobank resource with deep phenotyping and genomic data. *Nature*, 562(7726):203–209, 2018. doi: 10.1038/s41586-018-0579-z. URL https://doi.org/10.1038/s41586-018-0579-z.
- David Byrd and Antigoni Polychroniadou. Differentially private secure multi-party computation for federated learning in financial applications. In *Proceedings of the first ACM international conference on AI in finance*, pp. 1–9, 2020.
- Marco Cavallo and Çağatay Demiralp. A visual interaction framework for dimensionality reduction based data exploration. In *Proceedings of the 2018 CHI conference on human factors in computing systems*, pp. 1–13, 2018.
- Sebastian Damrich and Fred A Hamprecht. On umap's true loss function. *Advances in Neural Information Processing Systems*, 34:5798–5809, 2021.
- Sebastian Damrich, Jan Niklas Böhm, Fred A. Hamprecht, and Dmitry Kobak. From *t*-sne to umap with contrastive learning, 2023. URL https://arxiv.org/abs/2206.01816.
- Jan De Leeuw. Convergence of the majorization method for multidimensional scaling. *Journal of classification*, 5(2):163–180, 1988.

- Jan De Leeuw. Applications of convex analysis to multidimensional scaling. , ():, 2005.
 - Li Deng. The mnist database of handwritten digit images for machine learning research. *IEEE Signal Processing Magazine*, 29(6):141–142, 2012.
 - Carmelo Di Franco, Enrico Bini, Mauro Marinoni, and Giorgio C Buttazzo. Multidimensional scaling localization with anchors. In 2017 IEEE International Conference on Autonomous Robot Systems and Competitions (ICARSC), pp. 49–54, , 2017. IEEE, .
 - Chris Ding, Xiaofeng He, Hongyuan Zha, and Horst D Simon. Adaptive dimension reduction for clustering high dimensional data. In *2002 IEEE International Conference on Data Mining*, *2002. Proceedings.*, pp. 147–154. IEEE, 2002.
 - Petros Drineas, Asif Javed, Malik Magdon-Ismail, Gopal Pandurangan, Reino Virrankoski, and Andreas Savvides. Distance matrix reconstruction from incomplete distance information for sensor network localization. In 2006 3rd Annual IEEE Communications Society on Sensor and Ad Hoc Communications and Networks, volume 2, pp. 536–544. IEEE, 2006.
 - Cynthia Dwork, Frank McSherry, Kobbi Nissim, and Adam Smith. Calibrating noise to sensitivity in private data analysis. In *Theory of cryptography conference*, pp. 265–284. Springer, 2006.
 - Cynthia Dwork, Aaron Roth, et al. The algorithmic foundations of differential privacy. *Foundations and trends*® *in theoretical computer science*, 9(3–4):211–407, 2014.
 - Hilmi E Egilmez, Eduardo Pavez, and Antonio Ortega. Graph learning from data under laplacian and structural constraints. *IEEE Journal of Selected Topics in Signal Processing*, 11(6):825–841, 2017.
 - Bertrand T Fang. Trilateration and extension to global positioning system navigation. *Journal of Guidance, Control, and Dynamics*, 9(6):715–717, 1986.
 - Matt Fredrikson, Somesh Jha, and Thomas Ristenpart. Model inversion attacks that exploit confidence information and basic countermeasures. In *Proceedings of the 22nd ACM SIGSAC conference on computer and communications security*, pp. 1322–1333, 2015.
 - Matthew Fredrikson, Eric Lantz, Somesh Jha, Simon Lin, David Page, and Thomas Ristenpart. Privacy in pharmacogenetics: An {End-to-End} case study of personalized warfarin dosing. In 23rd USENIX security symposium (USENIX Security 14), pp. 17–32, 2014.
 - Dazhi Fu, Zhao Zhang, and Jicong Fan. Dense projection for anomaly detection. In *Proceedings of the AAAI Conference on Artificial Intelligence*, volume 38, pp. 8398–8408, 2024.
 - Octavian-Eugen Ganea, Gary Bécigneul, and Thomas Hofmann. Hyperbolic neural networks, 2018. URL https://arxiv.org/abs/1805.09112.
 - Jonas Geiping, Hartmut Bauermeister, Hannah Dröge, and Michael Moeller. Inverting gradients-how easy is it to break privacy in federated learning? *Advances in neural information processing systems*, 33:16937–16947, 2020.
 - Waldemar Gerok, Stefan Galler, and Thomas Kaiser. A novel approach to the mirroring problem in localization. In *2009 IEEE International Conference on Ultra-Wideband*, pp. 140–144. IEEE, 2009.
 - Felipe O. Giuste and Juan C. Vizcarra. Cifar-10 image classification using feature ensembles, 2020. URL https://arxiv.org/abs/2002.03846.
 - Oded Goldreich. Secure multi-party computation. *Manuscript. Preliminary version*, 78(110):1–108, 1998.
 - Yunhui Guo, Haoran Guo, and Stella Yu. Co-sne: Dimensionality reduction and visualization for hyperbolic data, 2022. URL https://arxiv.org/abs/2111.15037.
 - Andrew Hard, Kanishka Rao, Rajiv Mathews, Swaroop Ramaswamy, Françoise Beaufays, Sean Augenstein, Hubert Eichner, Chloé Kiddon, and Daniel Ramage. Federated learning for mobile keyboard prediction, 2019. URL https://arxiv.org/abs/1811.03604.

- Kaiming He, Xiangyu Zhang, Shaoqing Ren, and Jian Sun. Deep residual learning for image recognition. In *Proceedings of the IEEE conference on computer vision and pattern recognition*, pp. 770–778, 2016.
 - Samudra Herath, Matthew Roughan, and Gary Glonek. High performance out-of-sample embedding techniques for multidimensional scaling. *arXiv* preprint arXiv:2111.04067, 2021.
 - Hans Hofmann. Statlog (German Credit Data). UCI Machine Learning Repository, 1994. DOI: https://doi.org/10.24432/C5NC77.
 - M Hou. Uniqueness and hyperconic geometry of positioning with biased distance measurements. *GPS Solutions*, 26(3):79, 2022.
 - Peter A Iannucci, Lakshay Narula, and Todd E Humphreys. Cross-modal localization: Using automotive radar for absolute geolocation within a map produced with visible-light imagery. 2020.
 - Hyeon Jeon, Hyung-Kwon Ko, Jaemin Jo, Youngtaek Kim, and Jinwook Seo. Measuring and explaining the inter-cluster reliability of multidimensional projections. *IEEE Transactions on Visualization and Computer Graphics*, 28(1):551–561, 2021.
 - Alistair E. W. Johnson, Tom J. Pollard, Lu Shen, Li-wei H. Lehman, Mengling Feng, Mohammad Ghassemi, Benjamin Moody, Peter Szolovits, Leo Anthony Celi, and Roger G. Mark. Mimic-iii, a freely accessible critical care database. *Scientific Data*, 3(1):160035, 2016. doi: 10.1038/sdata. 2016.35. URL https://doi.org/10.1038/sdata.2016.35.
 - Ian T Jolliffe and Jorge Cadima. Principal component analysis: a review and recent developments. *Philosophical transactions of the royal society A: Mathematical, Physical and Engineering Sciences*, 374(2065):20150202, 2016.
 - Peter Kairouz, H Brendan McMahan, Brendan Avent, Aurélien Bellet, Mehdi Bennis, Arjun Nitin Bhagoji, Kallista Bonawitz, Zachary Charles, Graham Cormode, Rachel Cummings, et al. Advances and open problems in federated learning. *Foundations and trends® in machine learning*, 14(1–2):1–210, 2021.
 - Ravi Kannan. The frobenius problem. In Foundations of Software Technology and Theoretical Computer Science: Ninth Conference, Bangalore, India December 19–21, 1989 Proceedings 9, pp. 242–251. Springer, 1989.
 - Mohit Kataria, Sandeep Kumar, and Jayadeva. Ugc: Universal graph coarsening. In A. Globerson, L. Mackey, D. Belgrave, A. Fan, U. Paquet, J. Tomczak, and C. Zhang (eds.), *Advances in Neural Information Processing Systems*, volume 37, pp. 63057–63081. Curran Associates, Inc., 2024. URL https://proceedings.neurips.cc/paper_files/paper/2024/file/733209a1f12071a7ec979e8ffaeb1d99-Paper-Conference.pdf.
 - Martin Keller-Ressel and Stephanie Nargang. Strain-minimizing hyperbolic network embeddings with landmarks, 2022. URL https://arxiv.org/abs/2207.06775.
 - Usman A Khan, Soummya Kar, and José MF Moura. Distributed sensor localization in random environments using minimal number of anchor nodes. *IEEE Transactions on Signal Processing*, 57(5):2000–2016, 2009.
 - Moses A. Koledoye, Tullio Facchinetti, and Luis Almeida. Mds-based localization with known anchor locations and missing tag-to-tag distances. In 2017 22nd IEEE International Conference on Emerging Technologies and Factory Automation (ETFA), pp. 1–4, 2017. doi: 10.1109/ETFA. 2017.8247768.
 - Ya Le and Xuan S. Yang. Tiny imagenet visual recognition challenge. 2015.
- Liunian Harold Li, Patrick H. Chen, Cho-Jui Hsieh, and Kai-Wei Chang. Efficient contextual representation learning with continuous outputs. *Transactions of the Association for Computational Linguistics*, 7:611–624, 2019. doi: 10.1162/tacl_a_00289. URL https://aclanthology.org/Q19-1039/.

- Ziwei Li, Xiaoqi Wang, Hong-You Chen, Han-Wei Shen, and Wei-Lun Chao. Fedne: Surrogate-assisted federated neighbor embedding for dimensionality reduction, 2024. URL https://arxiv.org/abs/2409.11509.
- Leo Liberti, Carlile Lavor, Nelson Maculan, and Antonio Mucherino. Euclidean distance geometry and applications. *SIAM review*, 56(1):3–69, 2014.
- Samuel Lichtenberg and Abiy Tasissa. A dual basis approach to multidimensional scaling, 2024a. URL https://arxiv.org/abs/2303.05682.
- Samuel Lichtenberg and Abiy Tasissa. Localization from structured distance matrices via low-rank matrix recovery. *IEEE Transactions on Information Theory*, 2024b.
- Wei Yang Bryan Lim, Nguyen Cong Luong, Dinh Thai Hoang, Yutao Jiao, Ying-Chang Liang, Qiang Yang, Dusit Niyato, and Chunyan Miao. Federated learning in mobile edge networks: A comprehensive survey. *IEEE communications surveys & tutorials*, 22(3):2031–2063, 2020.
- Monika Litviňuková, Carlos Talavera-López, Henrike Maatz, Daniel Reichart, Catherine L. Worth, Eric L. Lindberg, Masatoshi Kanda, Krzysztof Polanski, Matthias Heinig, Michael Lee, Emily R. Nadelmann, Kenny Roberts, Liz Tuck, Eirini S. Fasouli, Daniel M. DeLaughter, Barbara McDonough, Hiroko Wakimoto, Joshua M. Gorham, Sara Samari, Krishnaa T. Mahbubani, Kourosh Saeb-Parsy, Giannino Patone, Joseph J. Boyle, Hongbo Zhang, Hao Zhang, Anissa Viveiros, Gavin Y. Oudit, Omer Ali Bayraktar, J. G. Seidman, Christine E. Seidman, Michela Noseda, Norbert Hubner, and Sarah A. Teichmann. Cells of the adult human heart. *Nature*, 588(7838): 466–472, 2020. doi: 10.1038/s41586-020-2797-4. URL https://doi.org/10.1038/s41586-020-2797-4.
- Nikita Malik, Rahul Gupta, and Sandeep Kumar. Hyperdefender: A robust framework for hyperbolic gnns. *Proceedings of the AAAI Conference on Artificial Intelligence*, 39(18):19396–19404, Apr. 2025. doi: 10.1609/aaai.v39i18.34135. URL https://ojs.aaai.org/index.php/AAAI/article/view/34135.
- Kanti V. Mardia and Anthony D. Riley. The classical multidimensional scaling revisited, 2021. URL https://arxiv.org/abs/2112.14503.
- Leland McInnes, John Healy, and James Melville. Umap: Uniform manifold approximation and projection for dimension reduction, 2020. URL https://arxiv.org/abs/1802.03426.
- Brendan McMahan, Eider Moore, Daniel Ramage, Seth Hampson, and Blaise Aguera y Arcas. Communication-efficient learning of deep networks from decentralized data. In *Artificial intelligence and statistics*, pp. 1273–1282. PMLR, 2017.
- Bamdev Mishra, Gilles Meyer, and Rodolphe Sepulchre. Low-rank optimization for distance matrix completion. In 2011 50th IEEE Conference on Decision and Control and European Control Conference, pp. 4455–4460. IEEE, 2011.
- Kevin R. Moon, David van Dijk, Zheng Wang, Scott Gigante, Daniel B. Burkhardt, William S. Chen, Kristina Yim, Antonia van den Elzen, Matthew J. Hirn, Ronald R. Coifman, Natalia B. Ivanova, Guy Wolf, and Smita Krishnaswamy. Visualizing structure and transitions for biological data exploration. *bioRxiv*, 2019. doi: 10.1101/120378. URL https://www.biorxiv.org/content/early/2019/04/04/120378.
- Milad Nasr, Reza Shokri, and Amir Houmansadr. Comprehensive privacy analysis of deep learning: Passive and active white-box inference attacks against centralized and federated learning. In 2019 IEEE symposium on security and privacy (SP), pp. 739–753. IEEE, 2019.
- Yuval Netzer, Tao Wang, Adam Coates, Alessandro Bissacco, Baolin Wu, Andrew Y Ng, et al. Reading digits in natural images with unsupervised feature learning. In *NIPS workshop on deep learning and unsupervised feature learning*, volume 2011, pp. 7. Granada, 2011.
- Hieu V Nguyen and Li Bai. Cosine similarity metric learning for face verification. In *Asian conference on computer vision*, pp. 709–720. Springer, 2010.

- Maximillian Nickel and Douwe Kiela. Poincaré embeddings for learning hierarchical representations. *Advances in neural information processing systems*, 30, 2017.
- Howard S Oster, Simon Crouch, Alexandra Smith, Ge Yu, Bander Abu Shrkihe, Shoham Baruch, Albert Kolomansky, Jonathan Ben-Ezra, Shachar Naor, Pierre Fenaux, et al. A predictive algorithm using clinical and laboratory parameters may assist in ruling out and in diagnosing mds. *Blood advances*, 5(16):3066–3075, 2021.
- Sebastian Pape and Kai Rannenberg. Applying privacy patterns to the internet of things'(iot) architecture. *Mobile Networks and Applications*, 24:925–933, 2019.
- Dong Qiao, Chris Ding, and Jicong Fan. Federated spectral clustering via secure similarity reconstruction. *Advances in Neural Information Processing Systems*, 36:58520–58555, 2023.
- Dong Qiao, Xinxian Ma, and Jicong Fan. Federated t-sne and umap for distributed data visualization, 2024. URL https://arxiv.org/abs/2412.13495.
- Aviv Regev, Sarah A Teichmann, Eric S Lander, Ido Amit, Christophe Benoist, Ewan Birney, Bernd Bodenmiller, Peter Campbell, Piero Carninci, Menna Clatworthy, Hans Clevers, Bart Deplancke, Ian Dunham, James Eberwine, Roland Eils, Wolfgang Enard, Andrew Farmer, Lars Fugger, Berthold Göttgens, Nir Hacohen, Muzlifah Haniffa, Martin Hemberg, Seung Kim, Paul Klenerman, Arnold Kriegstein, Ed Lein, Sten Linnarsson, Emma Lundberg, Joakim Lundeberg, Partha Majumder, John C Marioni, Miriam Merad, Musa Mhlanga, Martijn Nawijn, Mihai Netea, Garry Nolan, Dana Pe'er, Anthony Phillipakis, Chris P Ponting, Stephen Quake, Wolf Reik, Orit Rozenblatt-Rosen, Joshua Sanes, Rahul Satija, Ton N Schumacher, Alex Shalek, Ehud Shapiro, Padmanee Sharma, Jay W Shin, Oliver Stegle, Michael Stratton, Michael J T Stubbington, Fabian J Theis, Matthias Uhlen, Alexander van Oudenaarden, Allon Wagner, Fiona Watt, Jonathan Weissman, Barbara Wold, Ramnik Xavier, Nir Yosef, and Human Cell Atlas Meeting Participants. Science forum: The human cell atlas. *eLife*, 6:e27041, dec 2017. ISSN 2050-084X. doi: 10.7554/eLife.27041. URL https://doi.org/10.7554/eLife.27041.
- Nicola Rieke, Jonny Hancox, Wenqi Li, Fausto Milletari, Holger R Roth, Shadi Albarqouni, Spyridon Bakas, Mathieu N Galtier, Bennett A Landman, Klaus Maier-Hein, et al. The future of digital health with federated learning. *NPJ digital medicine*, 3(1):119, 2020.
- Alireza Vafaei Sadr, Bruce A Bassett, and Martin Kunz. A flexible framework for anomaly detection via dimensionality reduction. In 2019 6th International Conference on Soft Computing & Machine Intelligence (ISCMI), pp. 106–110. IEEE, 2019.
- Debbrata K Saha, Vince D Calhoun, Sandeep R Panta, and Sergey M Plis. See without looking: joint visualization of sensitive multi-site datasets. In *IJCAI*, pp. 2672–2678, 2017.
- Debbrata Kumar Saha, Vince Calhoun, Soo Min Kwon, Anand Sarwate, Rekha Saha, and Sergey Plis. Federated, fast, and private visualization of decentralized data. In *Federated Learning and Analytics in Practice: Algorithms, Systems, Applications, and Opportunities*.
- James B Saxe. Embeddability of weighted graphs in k-space is strongly np-hard. In *17th Allerton Conf. Commun. Control Comput.*, *1979*, pp. 480–489, 1979.
- Philip Sedgwick. Pearson's correlation coefficient. *Bmj*, 345, 2012.
- Yi Shang and Wheeler Ruml. Improved mds-based localization. In *IEEE INFOCOM 2004*, volume 4, pp. 2640–2651. IEEE, 2004.
- Micah J Sheller, G Anthony Reina, Brandon Edwards, Jason Martin, and Spyridon Bakas. Multiinstitutional deep learning modeling without sharing patient data: A feasibility study on brain tumor segmentation. In *Brainlesion: Glioma, Multiple Sclerosis, Stroke and Traumatic Brain Injuries: 4th International Workshop, BrainLes 2018, Held in Conjunction with MICCAI 2018, Granada, Spain, September 16, 2018, Revised Selected Papers, Part I 4*, pp. 92–104. Springer, 2019.
- Reza Shokri, Marco Stronati, Congzheng Song, and Vitaly Shmatikov. Membership inference attacks against machine learning models. In *2017 IEEE symposium on security and privacy (SP)*, pp. 3–18. IEEE, 2017.

- Carlos Oscar Sánchez Sorzano, Javier Vargas, and A Pascual Montano. A survey of dimensionality reduction techniques. *arXiv preprint arXiv:1403.2877*, 2014.
 - Latanya Sweeney. k-anonymity: A model for protecting privacy. *International journal of uncertainty, fuzziness and knowledge-based systems*, 10(05):557–570, 2002.
 - Abiy Tasissa and Rongjie Lai. Exact reconstruction of euclidean distance geometry problem using low-rank matrix completion. *IEEE Transactions on Information Theory*, 65(5):3124–3144, 2019. doi: 10.1109/TIT.2018.2881749.
 - Peter JG Teunissen. Carrier phase integer ambiguity resolution. In *Springer handbook of global navigation satellite systems*, pp. 661–685. Springer, 2017.
 - Laurens van der Maaten and Geoffrey Hinton. Visualizing data using t-sne. *Journal of Machine Learning Research*, 9(86):2579–2605, 2008. URL http://jmlr.org/papers/v9/vandermaaten08a.html.
 - Jarkko Venna and Samuel Kaski. Local multidimensional scaling with controlled tradeoff between trustworthiness and continuity. In *Proceedings of 5th Workshop on Self-Organizing Maps*, pp. 695–702, 2005.
 - Yansheng Wang, Yongxin Tong, and Dingyuan Shi. Federated latent dirichlet allocation: A local differential privacy based framework. In *Proceedings of the AAAI Conference on Artificial Intelligence*, volume 34, pp. 6283–6290, 2020.
 - Liu Wei, Dong En-qing, Zhang De-jing, et al. A new flip ambiguity detection algorithm in wireless networks node localization. *Acta Electron Sin*, 43(6):206–212, 2015.
 - Jiazhi Xia, Tianxiang Chen, Lei Zhang, Wei Chen, Yang Chen, Xiaolong Zhang, Cong Xie, and Tobias Schreck. Smap: A joint dimensionality reduction scheme for secure multi-party visualization. In 2020 IEEE Conference on Visual Analytics Science and Technology (VAST), pp. 107–118, 2020. doi: 10.1109/VAST50239.2020.00015.
 - Han Xiao, Kashif Rasul, and Roland Vollgraf. Fashion-mnist: a novel image dataset for benchmarking machine learning algorithms, 2017. URL https://arxiv.org/abs/1708.07747.
 - Jaewon Yang and Jure Leskovec. Defining and evaluating network communities based on ground-truth, 2012. URL https://arxiv.org/abs/1205.6233.
 - Jiancheng Yang, Rui Shi, Donglai Wei, Zequan Liu, Lin Zhao, Bilian Ke, Hanspeter Pfister, and Bingbing Ni. Medmnist v2 a large-scale lightweight benchmark for 2d and 3d biomedical image classification. *Scientific Data*, 10(1), January 2023. ISSN 2052-4463. doi: 10.1038/s41597-022-01721-8. URL http://dx.doi.org/10.1038/s41597-022-01721-8.
 - Andrew C Yao. Protocols for secure computations. In 23rd annual symposium on foundations of computer science (sfcs 1982), pp. 160–164. IEEE, 1982.
 - Huan Zhang, Yulong Liu, and Hong Lei. Localization from incomplete euclidean distance matrix: Performance analysis for the svd–mds approach. *IEEE Transactions on Signal Processing*, 67(8): 2196–2209, 2019.
 - Yue Zhao, Meng Li, Liangzhen Lai, Naveen Suda, Damon Civin, and Vikas Chandra. Federated learning with non-iid data. 2018. doi: 10.48550/ARXIV.1806.00582. URL https://arxiv.org/abs/1806.00582.
 - Ligeng Zhu, Zhijian Liu, and Song Han. Deep leakage from gradients. *Advances in neural information processing systems*, 32, 2019.

A APPENDIX

A.1 NEIGHBOR EMBEDDING (NE).

Definition A.1 t-SNE models p_{ij} as symmetrized conditional probabilities using Gaussian kernels: $p_{j|i} \propto \exp(-\|x_i - x_j\|^2/2\sigma_i^2)$, with $p_{ij} = \frac{p_{j|i} + p_{i|j}}{2n}$. Low-dimensional similarities are computed using a heavy-tailed Student-t kernel: $q_{ij} \propto (1 + \|y_i - y_j\|^2)^{-1}$. The loss minimizes the KL divergence:

$$\mathcal{L}_{\textit{tSNE}} = \sum_{i \neq j} p_{ij} \log rac{p_{ij}}{q_{ij}}.$$

Definition A.2 UMAP defines $p_{j|i} = \exp(-(\|x_i - x_j\| - \rho_i)/\tau_i)$ using adaptive exponential kernels, where ρ_i is the local connectivity threshold. Symmetrized p_{ij} is computed via fuzzy set union. In the embedding space, $q_{ij} = (1 + a\|y_i - y_j\|^2)^{-b}$ with fixed parameters (a, b). The loss is a weighted binary cross-entropy:

$$\mathcal{L}_{\textit{UMAP}} = \sum_{i \neq j} \left[p_{ij} \log \frac{p_{ij}}{q_{ij}} + (1 - p_{ij}) \log \frac{1 - p_{ij}}{1 - q_{ij}} \right].$$

A.2 CONTRASTIVE NEIGHBOR EMBEDDING (CNE).

Definition A.3 Given a kNN graph, high-dimensional similarities are binary: $S_{ij}^{d_h} = 1$ if $x_j \in kNN(x_i)$, and 0 otherwise. In the embedding space, similarities are defined using a Cauchy kernel: $S_{ij}^{d_l} = \phi(\mathbf{y}_i, \mathbf{y}_j) = \frac{1}{1 + ||\mathbf{y}_i - \mathbf{y}_j||^2}$. The CNE objective combines attractive and repulsive forces:

$$\mathcal{L}(\theta) = -\mathbb{E}_{(i,j) \sim p_i} \log \phi(f_{\theta}(\mathbf{x}_i), f_{\theta}(\mathbf{x}_j)) - b\mathbb{E}_{(i,j)} \log(1 - \phi(f_{\theta}(\mathbf{x}_i), f_{\theta}(\mathbf{x}_j))),$$

where p_i samples positive pairs and b > 0 balances the repulsion term.

A.3 HYPERBOLIC MODELS AND DISTANCE CALCULATION.

There are several equivalent models of hyperbolic geometry exist, including the Poincaré ball model, lorentz model (or hyperboloid model) and the upper half-space model. The mathematical framework of the *d*-dimensional hyperboloid model of hyperbolic geometry is deined as follows:

For $x, y \in \mathbb{R}^{d+1}$, the Lorentz product is an indefinite inner product given by,

$$x \circ y := x_1 y_1 - (x_2 y_2 + \dots + x_{d+1} y_{d+1}). \tag{12}$$

The real vector space \mathbb{R}^{d+1} equipped with this inner product is called *Lorentz space*, denoted by $\mathbb{R}^{1,d}$. It contains the *positive Lorentz space* as a subset:

$$\mathbb{R}^{1,d}_+ := \left\{ x \in \mathbb{R}^{1,d} : x_1 > 0 \right\}.$$

Within $\mathbb{R}^{1,d}_+$, the *single-sheet hyperboloid* \mathbb{H}^{d_h} is given by

$$\mathbb{H}^{d_h} := \left\{ x \in \mathbb{R}^{1,d} : x \circ x = 1, \ x_1 > 0 \right\}. \tag{13}$$

The hyperboloid model in dimension d with curvature $-\kappa$ (for $\kappa > 0$) consists of \mathbb{H}^{d_h} endowed with the hyperbolic distance:

$$d_{\mathbb{H}}^{\kappa}(x,y) = \frac{1}{\sqrt{\kappa}}\operatorname{arcosh}(x \circ y), \quad x, y \in \mathbb{H}^{d_h}.$$
(14)

The distance $d_{\mathbb{H}}^{\kappa}$ is a valid metric on \mathbb{H}^{d_n} , it is positive definite and satisfies the triangle inequality. Moreover, equipped with the metric tensor:

$$ds^2 = \frac{1}{\kappa} (dx \circ dx),$$

the hyperboloid \mathbb{H}^{d_h} becomes a Riemannian manifold of constant sectional curvature $-\kappa$, and $d_{\mathbb{H}}^{\kappa}$ corresponds exactly to its geodesic distance. In particular, the curvature κ does not alter the definition of the manifold \mathbb{H}^{d_h} itself, but only scales the distance metric. Just as Euclidean space is the canonical model for zero curvature, hyperbolic space is the canonical geometry for constant negative curvature.

A.3.1 POINCARÉ BALL MODEL.

The Poincaré ball model is the most widely used formulation of hyperbolic space in machine learning (Nickel & Kiela, 2017; Ganea et al., 2018). It defines the n-dimensional hyperbolic space as $\mathbb{B}^n = \{x \in \mathbb{R}^n : \|x\| < 1\}$ with Riemannian metric $g_x = \left(\frac{2}{1-\|x\|^2}\right)^2 I_n$. The hyperbolic distance between two points $u, v \in \mathbb{B}^n$ is:

$$d_{\mathbb{B}^n}(u,v) = \operatorname{arcosh}\left(1 + \frac{2\|u - v\|^2}{(1 - \|u\|^2)(1 - \|v\|^2)}\right). \tag{15}$$

This distance increases exponentially near the boundary, enabling natural hierarchical embeddings where central points correspond to root nodes and peripheral points to leaves.

A.4 CO-SNE

Definition A.4 CO-SNE defines the similarities via hyperbolic normal kernels in the high-dimensional Poincaré ball \mathbb{B}^n : $p_{j|i} = \exp\left(-d_{\mathbb{B}^n}(x_i,x_j)^2/2\sigma_i^2\right)/Z_i$, with $p_{ij} = (p_{j|i}+p_{i|j})/2m$. In the embedding space \mathbb{B}^2 , similarities use a hyperbolic Cauchy kernel: $q_{ij} = \gamma^2/(d_{\mathbb{B}^2}(y_i,y_j)^2 + \gamma^2)/Z$. The loss combines KL divergence with a norm-based regularizer:

$$\mathcal{L}_{CO\text{-SNE}} = \lambda_1 \sum_{i,j} p_{ij} \log \frac{p_{ij}}{q_{ij}} + \lambda_2 \sum_{i} (\|x_i\|^2 - \|y_i\|^2)^2.$$
 (16)

A.5 CLASSICAL MDS

Utilizing the measurements of distances among pairs of objects, MDS (multidimensional scaling) finds a representation of each object in d - dimensional space such that the distances are preserved in the estimated configuration as closely as possible. To validate the goodness-of-fit measure, MDS optimizes the loss function (known as "Stress" (σ)) given by:

$$\sigma(X) = \min_{X} \sum_{i < j \le N} w_{ij} \left(\delta_{ij} - d_{ij}(X) \right)^2, \tag{17}$$

, where the observation mask is W where $w_{ij} = 1$ if the distance δ_{ij} is known and $w_{ij} = 0$ otherwise, with the block structure:

$$W = \begin{bmatrix} \mathbf{0}_{N \times N} & \mathbf{1}_{N \times M} \\ \mathbf{1}_{M \times N}^{\top} & \mathbf{1}_{M \times M} \end{bmatrix}$$
 (18)

where ${\bf 0}$ and ${\bf 1}$ denote matrices of zeros and ones, respectively and X represents the computed configuration, $d_{ij}(X) = \|{\bf x}_i - {\bf x}_j\|$ is the Euclidean distance between nodes i and j, δ_{ij} is the measured distance computed privately. Placing the weights of unknown inter-user distance to zero, the weight matrix W can be partitioned into block matrices as shown in 18, where $11_{N,M}$ is a matrix of ones with shape $N \times M$. De Leeuw (De Leeuw, 2005) applied an iterative method called SMACOF (Scaling by Majorizing a Convex Function) to estimate the configuration X. As the objective is a non-convex function, SMACOF minimizes the stress using the simple quadratic function $\tau(X,Z)$ which bounds $\sigma(X)$ (the complicated function) from above and meets the surface at the so-called supporting point Z as defined below:

$$\sigma(X) \le \tau(X, Z) = \sum_{i \le j} w_{ij} \delta_{ij}^2 + \sum_{i \le j} w_{ij} d_{ij}^2(X) - 2 \sum_{i \le j} w_{ij} \delta_{ij}^2 \frac{(\boldsymbol{x_i} - \boldsymbol{x_j})^T (\boldsymbol{z_i} - \boldsymbol{z_j})}{\|\boldsymbol{z_i} - \boldsymbol{z_j}\|}$$
(19)

Equation 19 can be written in matrix form as:

$$\tau(X,Z) = C + \operatorname{tr}\left(X^T V X\right) - 2\operatorname{tr}\left(X^T B(Z)Z\right). \tag{20}$$

The iterative solution which guarantees monotone convergence of stress (De Leeuw, 1988) is given by equation 21, where $Z = X^{k-1}$:

$$X^{(k)} = \min_{X} \tau(X, Z) = V^{\dagger} B(X^{(k-1)}) X^{(k-1)}$$
(21)

This algorithm offers flexibility to embed features in any dimension other than d, which enables the handling of high-dimensional data and also meets privacy constraints. As V is not of full rank, hence

the Moore-Penrose pseudoinverse V^{\dagger} is used. The elements of the matrix B(X) and V are defined in equation 22.

$$b_{ij} = \begin{cases} -\frac{w_{ij}\delta_{ij}}{d_{ij}(\mathbf{X})}, & \text{if } d_{ij}(\mathbf{X}) \neq 0, \ i \neq j \\ 0, & \text{if } d_{ij}(\mathbf{X}) = 0, \ i \neq j \\ -\sum_{j=1, \ j \neq i}^{N} b_{ij}, & \text{if } i = j \end{cases}$$

$$(22)$$

$$v_{ij} = \begin{cases} -w_{ij}, & \text{if } i \neq j \\ -\sum\limits_{j=1, j \neq i}^{N} v_{ij}, & \text{if } i = j \end{cases}$$

A.6 SENSE: PSEUDOCODE

Algorithm 1 SENSE Framework

Require: Anchors $\mathbf{X}_A \in \mathbb{R}^{K \times d_h}$, client datasets $\{\mathcal{D}_m = \{x_i^m\}_{i=1}^{N_m}\}_{m=1}^M$, target dim d_ℓ , high/low geometry $\mathbb{G}_{\text{high}} \in \{\mathbb{R}^{d_{\text{h}}}, \mathbb{H}^{d_{\text{h}}}\}, \mathbb{G}_{\text{low}} \in \{\mathbb{R}^{d_{\ell}}, \mathbb{H}^{d_{\ell}}\}$

Ensure: Global embeddings $\{\mathbf{Y}^m \in \mathbb{G}_{\text{low}}^{N_m}\}_{m=1}^M$

- 1: Server broadcasts X_A to all clients
- 2: **for** each client C_m **do**
- Compute distances $\mathbf{d}_i^m = \mathcal{D}_{\mathbb{G}_{\text{high}}}(x_i^m, \mathbf{X}_A)$ for all $x_i^m \in \mathcal{D}_m$ Send $\{\mathbf{d}_i^m\}_{i=1}^{N_m}$ to server
- 4:

918

919

920

925 926

931 932

933

934

935

936

937

938 939

940 941

942

943

944

945 946

947

948 949

950

951

952 953

954 955

956

957

958 959

960

961 962

963

964

965

966

967

968

969

970

971

- 6: Server builds observed matrix \mathbf{D}_{Ω} using E, F, (optionally G)
- 7: Complete $\hat{\mathbf{D}}$ via structured matrix completion; extract $\hat{\mathbf{G}}$
- 8: Compute similarities S^{d_h} from $\hat{\mathbf{G}}$ using kernel f (see Eqns 6, 7)
- 9: Learn embedding Y in \mathbb{G}_{low} using NE, contrastive, or CO-SNE objective

SENSE VIA ANCHORED-MDS: PSEUDOCODE

Algorithm 2 SENSE via Anchored-MDS

Require: Anchor embeddings $X_A \in \mathbb{R}^{K \times d_h}$, observed entries $\mathcal{P}_{\Omega}(D)$, target dim d_h , tolerance ϵ , max iterations T

Ensure: Reconstructed embeddings $X_{NA} \in \mathbb{R}^{N \times d_h}$

- 1: Initialize $X_{NA}^{(0)}$ randomly, set $k \leftarrow 1$ 2: **while** $k \leq T$ **do**
- Form $X^{(k-1)} = \begin{bmatrix} X_A & X_{NA}^{(k-1)} \end{bmatrix}^T$
- Compute $\mathcal{P}_{\Omega}(D(X^{(k-1)}))$ 4:
- Construct W and compute $V, B(X^{(k-1)})$ respecting Ω
- Update $X_{NA}^{(k)}$ using Eq. 11 If stress improvement $<\epsilon$, **break**; else $k\leftarrow k+1$
- 8: end while
- 9: **return** $X_{NA}^{(\kappa)}$

ANCHOR GENERATION

In the proposed method, distribution of the anchor data is critical. These anchors are not private; they act as public or semi-public landmarks, akin to those in GPS (Shang & Ruml, 2004) or radar systems (Iannucci et al., 2020). This is standard in localization literature (Di Franco et al., 2017; Khan et al., 2009), where landmarks aid positioning but are not privacy-sensitive (Koledoye et al., 2017). Our privacy definition protects only the high-dimensional features of NA points. Anchors are fixed, visible, and either synthetic, public, or explicitly consented. Not part of any client's private data. We do not rely on anchor secrecy but instead limit their quantity to preserve ambiguity.

The anchor is a common information shared between all the clients. The anchor data is generated randomly or by open data for securing privacy. The proper scheduling of the anchors has a significant

impact on the overall performance and accuracy of the framework. There are several factors to consider when developing the anchor scheduling strategy, including:

1) **Number of anchors**: The number of anchors used in the framework has a direct impact on the algorithmic performance. Too few anchors may not preserve the structural information while ensuring privacy, while too many anchors may violate privacy.

Choice of K: We sample anchors such that the total (global + local) anchors satisfy $K = d_h - 1$, where d_h is the input dimension. This is not arbitrary; it is *theoretically optimal* under our privacy guarantee. By Theorem 3.1, if $K < d_h$, privacy is ensured. Thus, $K = d_h - 1$ is the largest safe choice that preserves privacy while still yielding strong approximations. There is an inherent privacy-utility-compute trade-off:

- 1. Higher *K*: better fidelity, higher runtime, weaker privacy.
- 2. Lower *K*: stronger privacy, lower compute cost, possible fidelity drop.

We empirically validate this trade-off on a synthetic dataset where we took K anchors and N NA points in a pointwise setting with d_h dimension.

For low-dimensional data ($d_h = 100, N = 500$):

```
• K = 99 \Rightarrow FS = 0.79, time = 16s
```

•
$$K = 90 \implies FS = 0.78$$
, time = 13s

For high-dimensional data ($d_h = 700, N = 500$):

```
• K = 699 \implies FS = 0.82, time = 660s
```

•
$$K = 350 \implies FS = 0.78$$
, time = 312s

Thus, for high-dimensional settings where $d_h \gg N$, using fewer anchors (e.g., $K < d_h - 1$) yields substantial computational gains while preserving utility. This is particularly useful in large-scale deployments such as hospital networks, financial networks, social media platforms and IOT networks.

2) Anchor Geometry: Beyond count, anchor geometry also impacts fidelity. We show that affinely independent anchors improve reconstruction quality. On the DIGITS dataset $(N=1797, d_h=64)$ (Alpaydin & Kaynak, 1998), we fixed K=63 and varied the anchor matrix rank r. The non-anchor set consisted of 1000 points, split across 10 clients (multisite-full). Table 4 validates that higher affine rank of anchors improves neighborhood fidelity, consistent with our theory.

Table 4: Effect of anchor matrix rank r on FS and DE in the DIGITS dataset (K=63). Higher rank improves fidelity.

\overline{r}	FS	DE
10	0.524	0.0829
20	0.6242	0.0604
30	0.716	0.0479
40	0.7955	0.0361
50	0.8315	0.0311
60	0.858	0.0259
63	0.861	0.0263

- **3) Selection criteria**: The criteria used to select anchors can also impact the performance of the system. Selecting anchors from the same probability distribution as of the underlying user data may be more effective than selecting them at random. For example, the data distribution of patient similarity networks or social networks will depend on factors including a number of patients/users or similarity of patients/connection between users. We also empirically study how anchor selection affects downstream performance. Random anchor sampling performs worse than anchors sampled from the underlying data distribution. Table 5 confirms that *in-distribution anchors preserve structure better*. Setup: 10 clients, 1000 non-anchor points, multisite-full setting.
- **4) Practical Anchor Sources.** In practical deployments, anchors are selected based on domain knowledge and are not sampled arbitrarily from private data. Eg, Healthcare: Publicly released

Table 5: Effect of anchor selection on fidelity (FS) and distance error (DE). In-distribution anchors outperform random anchors across datasets.

Data	Anchor-Type	K	FS	DE
Digits	In-Distri	60	0.900	0.027
	Rand	60	0.345	0.382
MNIST	In-Distri	783	0.967	0.006
	Rand	783	0.170	0.602
BloodMNIST	In-Distri	2351	0.961	0.005
	Rand	2351	0.176	0.892

reference scans or patient-consented samples (Johnson et al., 2016). Finance: Standard transaction patterns or aggregated customer profiles (Awosika et al., 2024b). Genomics: Population-level reference genomes (e.g., 1000 Genomes, UK Biobank) (Bycroft et al., 2018; Regev et al., 2017). Synthetic Anchors: Via MMD minimization (Qiao et al., 2024), though limited in coverage and potentially adversarial. Trusted server-curated anchors are auditable, robust, and independent of client records, reducing leakage risks like membership inference (Shokri et al., 2017). This design is further supported by theory on low-rank recovery via anchor distances (Lichtenberg & Tasissa, 2024b), matrix completion in non-orthogonal bases (Tasissa & Lai, 2019), and Gram matrix-based localization (Mishra et al., 2011).

Table 6: Observed index sets Ω used for SENSE under each client configuration. Here, \mathcal{A}_G denotes global anchors, $\mathcal{A}_L^{(j)}$ are local anchors accessible only to client j, and $\mathcal{X}^{(m)}$ are NA indices at client m. Binary masks W_F and W_G indicate anchor-to-NA and intra-client NA–NA visibility. Observed distances are used to construct V, B(X), and select relevant rows of X_A for embedding computation.

SENSE Setting	Observed Index Set Ω
Pointwise-Full	Each client holds one NA. All anchor-to-NA distances are known; no NA–NA or local anchor information. $\Omega = \{(i,j): i \in \mathcal{A}_G, \ j \in [K+1,K+N]\} \cup \{(j,i): i \in \mathcal{A}_G, \ j \in [K+1,K+N]\}$
Pointwise-Partial	Each client holds one NA. Global anchors \mathcal{A}_G are shared across all clients. Local anchors $\mathcal{A}_L^{(j)}$ are only accessible to client j . $\Omega = \bigcup_{j=1}^N \left((\mathcal{A}_G \cup \mathcal{A}_L^{(j)}) \times \{K+j\} \cup \{K+j\} \times (\mathcal{A}_G \cup \mathcal{A}_L^{(j)}) \right)$
Multisite-Full	Each client holds multiple NAs. All anchor-to-NA distances are known. Intraclient NA–NA distances are observed. $\Omega = \{(i,j): i \in \mathcal{A}_G, j \in [K+1,K+N]\} \cup \{(j,i): i \in \mathcal{A}_G, j \in [K+1,K+N]\} \cup \bigcup_{m=1}^M (\mathcal{X}^{(m)} \times \mathcal{X}^{(m)})$
Multisite-Partial	Each client holds multiple NAs. Anchor-to-NA distances are partially known via W_F (global + local anchors). Intra-client NA–NA distances are observed via W_G . $\Omega = \{(i,j+K): W_F[i,j]=1\} \cup \{(j+K,i): W_F[i,j]=1\} \cup \{(i,j): W_G[i,j]=1\}$

A.9 THEORETICAL PROOFS.

Unlike some EDG (Tasissa & Lai, 2019) methods that assume uniform random sampling of pairwise distances, SENSE uses a structured sampling scheme where anchor-to-NA distances are measured by design. This enables deterministic recovery guarantees based on geometric conditions (e.g., connectivity to affinely independent anchors), avoiding reliance on probabilistic bounds from random sampling.

Proof A.1 Consider a network in d_h -dimensional Euclidean space \mathbb{R}^{d_h} , comprising anchors $A = \{A_1, A_2, \ldots, A_K\}$ and non-anchor nodes $P = \{P_1, P_2, \ldots, P_N\}$, with feature vectors $\mathbf{x_i} \in \mathbb{R}^{d_h}$. Anchors locations are known, while non-anchors need estimation. Previous work (Khan et al., 2009) shows that in \mathbb{R}^{d_h} , a minimum of (d+1) anchors with known locations is required to locate N non-anchor nodes. The utilization of anchors for distributed sensor localization constitutes a thoroughly investigated domain, underpinned by the following assumptions:

- (A1) Non-anchor nodes lie inside the convex hull of the anchors, i.e., $C(P) \subseteq C(A)$.
- (A2) Each non-anchor node P_i has at least one set of neighbor nodes $N_i \subset (A \cup P)$ with $|N_i| = d_h + 1$ such that i lies inside $C(N_i)$.
- (A3) In the set $\{i \cup N_i\}$, every non-anchor node i can obtain the inter-node distances among all nodes.

However, to accurately recover features in \mathbb{R}^{d_h} , at least d_h anchors are necessary, even if non-anchors are placed in any location. Thus, having fewer than d_h anchors, i.e., $K < d_h$, guarantees that exact feature embeddings cannot be obtained, ensuring privacy.

Proof A.2 Each NA point $x_j \in \mathbb{R}^{d_h}$ computes squared distances to a subset of anchors indexed by \mathcal{I}_j , with $r_j = |\mathcal{I}_j|$. This yields r_j quadratic constraints of the form:

$$\|\boldsymbol{x}_j - \boldsymbol{a}_i\|^2 = d_{hij}^2, \quad \forall i \in \mathcal{I}_j.$$

To analyze identifiability, fix a reference anchor $a_k \in \mathcal{I}_G$ from the global anchor set, and consider the difference of equations relative to this reference:

$$\|\boldsymbol{x}_{j} - \boldsymbol{a}_{i}\|^{2} - \|\boldsymbol{x}_{j} - \boldsymbol{a}_{k}\|^{2} = d_{hij}^{2} - d_{hkj}^{2}.$$

Expanding and simplifying yields the linear system:

$$2(a_k - a_i)^{\top} x_j = ||a_k||^2 - ||a_i||^2 + d_{hij}^2 - d_{hkj}^2, \quad \forall i \in \mathcal{I}_j \setminus \{k\}.$$

Letting $A_i \in \mathbb{R}^{(r_j-1)\times d}$ denote the coefficient matrix and b_i the RHS vector, we write:

$$A_i \boldsymbol{x}_i = \boldsymbol{b}_i.$$

This is a system of $r_j - 1$ linear equations in d_h unknowns. If $r_j < d_h + 1$, then $rank(A_j) \le r_j - 1 < d_h$, and the solution set $\{x_j \in \mathbb{R}^{d_h} : A_j x_j = b_j\}$ forms an affine subspace of dimension at least $d_h - r_j + 1$. Hence, infinitely many solutions exist that satisfy the same anchor distances, preventing exact recovery of x_j .

To ensure privacy across all clients (both pointwise and multisite), we enforce:

$$|\mathcal{I}_j| = K_G + K_L^{(j)} \le d_h, \quad \forall j \in [N],$$

where $K_L^{(j)}$ is the number of local anchors accessible to x_j . In the multisite case, local anchors are restricted to the corresponding client, and global anchors are common across all clients. This structure ensures that even with partial anchor visibility, each client's feature vector cannot be uniquely recovered from its observed distances.

Remark 3 Each anchor distance imposes a quadratic constraint on the unknown $x_j \in \mathbb{R}^{d_h}$. If the number of constraints r_j is less than the ambient dimension d, the system is underdetermined and has infinitely many solutions. Thus, SENSE preserves privacy by bounding the number of anchor distances accessible to each client.

Proof A.3 From Theorem 3.1 (Exact Recovery) in (Keller-Ressel & Nargang, 2022), the L-HYDRA algorithm guarantees recovery up to isometry only if $K \geq d_h$ and the K anchors are in general position (not lying on a single hyperbolic hyperplane). If $K < d_h$, then the system of equations defined by E and F is underdetermined: the landmarks do not span $\mathbb{H}_h^{d_h}$, and multiple embeddings of the NA points are consistent with the observed distances. Hence, SENSE ensures privacy by choosing $K < d_h$, preventing unique reconstruction of private client embeddings.

A.10 Why $K < d_h$ and not $K \le d_h$?

While both k < d and k = d can contribute to privacy, our choice of k < d is a deliberate design decision driven by the well-known mirror ambiguity problem (details in NOTE2) inherent in certain geometric transformations when k = d.

Why Choosing K < d Anchors is Better for Privacy than K = d: In distance-based reconstruction problems such as the Distance Geometry Problem (DGP) (Liberti et al., 2014), network localization (Lichtenberg & Tasissa, 2024b), or hyperbolic embedding recovery (Keller-Ressel & Nargang, 2022), the number and configuration of anchor points (i.e., known reference points with distance access to

an unknown point) directly affect how precisely an adversary can reconstruct the hidden point. From a privacy perspective, we aim to make the reconstruction problem ambiguous, so that the true point remains hidden among many plausible candidates. We argue that choosing K=D-1 (or fewer) anchors is preferable to choosing K=D, especially when protecting sensitive features such as location or identity (in case of hospital patients or other critical attributes). This relates to ambiguity, recoverability, and robustness under both Euclidean and hyperbolic regimes.

Case 1: K=D, Affinely Independent Anchors \rightarrow Small, Structured Ambiguity: When an adversary knows distances from an unknown point $x \in \mathbb{R}^D$ to D affinely independent anchors, the solution set for x becomes tightly constrained: The point lies on a 1D manifold, typically a circle (in 2D/3D). This is the intersection of D hyperspheres in \mathbb{R}^D , reducing degrees of freedom to 1 (rotation around the affine hull of the anchors). *Example:* In 2D: 2 non-collinear anchors \Rightarrow two symmetric positions across the anchor line. In 3D: 3 non-coplanar anchors \Rightarrow solution lies on a circle (Liberti et al., 2014) and also in (Liberti et al., 2014; Biswas & Ye, 2004; Fang, 1986). This is called *structured ambiguity*: the solution isn't unique, but the adversary can narrow it down to a small, reversible set, which weakens privacy. BUT: K = D Affinely Dependent Anchors \rightarrow Degeneracy Risk: If the D anchors are affinely dependent (e.g., lie on a hyperplane), the problem becomes ill-posed. The linear system degenerates, and the solution set can inflate from a curve to a surface or even higher. *Example:* In 2D: 2 collinear anchors \Rightarrow infinite feasible points on a circle. In 3D: 3 coplanar anchors \Rightarrow solution lies on a cylinder surface (2D ambiguity) (Liberti et al., 2014). Thus, while ambiguity helps privacy, this case is fragile and depends on affine dependence, which is difficult to control/detect in high dimensions.

Case 2: K = D - 1, Affinely Independent Anchors \rightarrow Robust, Structured Ambiguity: When the number of anchors is reduced to K = D - 1 and they are affinely independent: The intersection of D - 1 hyperspheres in \mathbb{R}^D leaves the unknown point on a 1D manifold (if K = D - 1) or a 2D manifold (if K = D - 2). This increases ambiguity while preserving structure and analyzability. *Example:* In 3D: 2 non-collinear anchors \Rightarrow solution lies on a sphere surface (2D ambiguity). In 4D: 3 anchors \Rightarrow solution lies on a 2D manifold in \mathbb{R}^4 (Liberti et al., 2014). *This ambiguity is independent of affine structure:* even with poorly placed anchors, ambiguity remains large enough to preserve privacy.

Case 3: Moreover, L-HYDRA Shows, $K \ge d$ Enables Exact Recovery \to Privacy Violation: In hyperbolic space, the L-HYDRA framework (Keller-Ressel & Nargang, 2022) (Theorem 3.1) shows that if $l \ge d$ well-placed landmarks are known, exact recovery up to isometry is possible. While useful for learning, this completely breaks privacy at K = d. Thus, in the SENSE framework, we limit the number of anchor constraints to prevent identifiability, ensure privacy, and make it more generic and applicable across all cases.

Why K = D - 1 is the safe design choice for privacy? We prefer using K = D - 1 anchors because:

- 1. *More Ambiguity = More Privacy:* Reducing constraints expands the feasible set (e.g., from a 1D curve to a 2D surface). This makes inference harder for an adversary.
- 2. Independent of Affine Structure: Unlike K=D, where affine dependence can create degeneracy, K=D-1 is robust regardless of anchor configuration.
- 3. *No Added Utility Beyond Isometry:* Recovering up to isometry is sufficient for many applications (e.g., visualization, clustering). Adding more anchors increases identifiability risk without improving downstream performance anymore.

Thus, choosing K < d affinely independent anchors is a principled design choice for privacy-preserving recovery. It: maximizes geometric ambiguity without losing structure, avoids degeneracy from affine dependence, and preserves robustness in both Euclidean and hyperbolic settings. In contrast, using K = D leads to tight constraints, small ambiguity, and easy inference, enabling potential attacks. Our design choice in SENSE and related frameworks deliberately limits anchor access to protect against such risks.

Note1: In decentralized or federated settings, adversaries aiming to reconstruct private data using techniques such as model inversion, membership inference, attribute inference, gradient leakage, or reconstruction attacks, gain a significant advantage when the solution space is small and structured (Fredrikson et al., 2015; Shokri et al., 2017; Fredrikson et al., 2014; Zhu et al., 2019; Geiping et al., 2020; Nasr et al., 2019). A constrained set of possible solutions (e.g., a one-dimensional curve or a

mirrored pair of points) reduces uncertainty, making it easier to link gradients or model updates back to the original data. Conversely, a larger and more ambiguous solution space (e.g., a high-dimensional manifold) introduces uncertainty and increases the difficulty of pinpointing a unique inverse mapping. In such cases, adversarial inference becomes more challenging, as multiple plausible candidates exist. Therefore, introducing geometric ambiguity—for instance, by designing the solution space such that K < d—can serve as an effective defense mechanism in privacy-sensitive scenarios. Also, non-uniqueness alone is not sufficient: we must consider how large, diverse, and unstructured the solution set is to ensure meaningful privacy.

Note2: The *mirror ambiguity problem* arises in localization when distances to a limited set of anchors admit multiple, equally valid solutions that are reflections of each other (Wei et al., 2015; Bose et al., 2017; Hou, 2022; Gerok et al., 2009; Betti et al., 1993; Teunissen, 2017; Saxe, 1979). This occurs especially when the number of anchors k equals the dimensionality d. For instance, in 2D with two anchors, the target point lies at the intersection of two circles, yielding two symmetric solutions across the anchor line; in 3D with three anchors, the solution lies on a mirrored circle. In wireless networks, this is referred to as *flip ambiguity*, where measurement noise exacerbates the uncertainty (Wei et al., 2015). Detecting such ambiguity is equivalent to finding a plane intersecting all error spheres of the anchors. The root cause is geometric: distance measurements lack directionality, and k = d anchors do not sufficiently constrain the solution, leading to mirror symmetry. Practical implications include localization errors and navigation failures in robotics and sensor networks. In graph-theoretic terms (Saxe, 1979), the problem corresponds to embedding a weighted graph (nodes as points, edges as distances) into k-space. When anchors equal the embedding dimension, the embedding is ambiguous up to reflections, producing multiple valid placements across a plane or hyperplane defined by the anchors.

A.11 METRIC USED.

• Cosine Similarity (CosSim): Measures angular similarity between the original NA feature matrix $X'_{NA} \in \mathbb{R}^{N \times d_h}$ and the reconstructed version $X_{NA} \in \mathbb{R}^{N \times d_h}$ from SENSE-anchored MDS. Cosine similarity is computed as:

$$CosSim(X'_{NA}, X_{NA}) = \frac{1}{N} \sum_{i=1}^{N} \frac{\langle (X'_{NA})^{(i)}, X_{NA}^{(i)} \rangle}{\|(X'_{NA})^{(i)}\| \cdot \|X_{NA}^{(i)}\|}$$

High values (close to 1) indicate strong alignment between original and reconstructed embeddings.

- Distance Error (DE): and F-score (FS): defined in Section 4.1.
- Pearson Correlation (ρ): Quantifies linear correlation between the original and reconstructed NA–NA distance matrices:

$$\rho = \text{Pearson}(G_{ij}, \widehat{G}_{ij}), \quad \forall i < j$$

where G and \widehat{G} denote the ground-truth and reconstructed distance matrices respectively. Values close to 1 indicate that the relative distance structure is preserved.

• Frobenius Norm Error (X_{frob}) : Measures reconstruction error in the embedding space:

$$X_{\text{frob}} = \frac{\|X_{\text{NA}} - X'_{\text{NA}}\|_F}{\|X'_{\text{NA}}\|_F}$$

A value of 0 implies perfect reconstruction; higher values suggest increasing deviation.

A.12 DATASET STATISTICS.

Table 7: Dataset statistics and learning setups grouped by embedding geometry. For hyperbolic, the stats are for *Pointwise* setting.

Space	Dataset	#Classes	#Datapoints	#Clients (M)	Dimension
	MNIST	10	25000	10	784
	Fashion-MNIST	10	25000	10	784
	CIFAR-10	10	25000	5/10	1024
	DermaMNIST	7	10015	10	784
	PneumoniaMNIST	2	5856	10	784
Euclidean	RetinaMNIST	5	1600	10	784
	BreastMNIST	2	780	10	784
	BloodMNIST	8	17092	10	784
	OrganCMNIST	11	23583	10	784
	OrganSMNIST	11	25211	10	784
	German-Credit	2	1000	10	20
	Airport	4	3185	3185	11
Hyperbolic	Amazon	-	5000	5000	128
	DBLP	-	5000	5000	128

A.13 SYSTEM SPECIFICATIONS

All experiments are conducted on a server equipped with two **NVIDIA RTX A6000** GPUs (48 GB memory each) and an **Intel Xeon Platinum 8360Y** CPU with **1 TB RAM**.

A.14 VISUALIZATION RESULTS

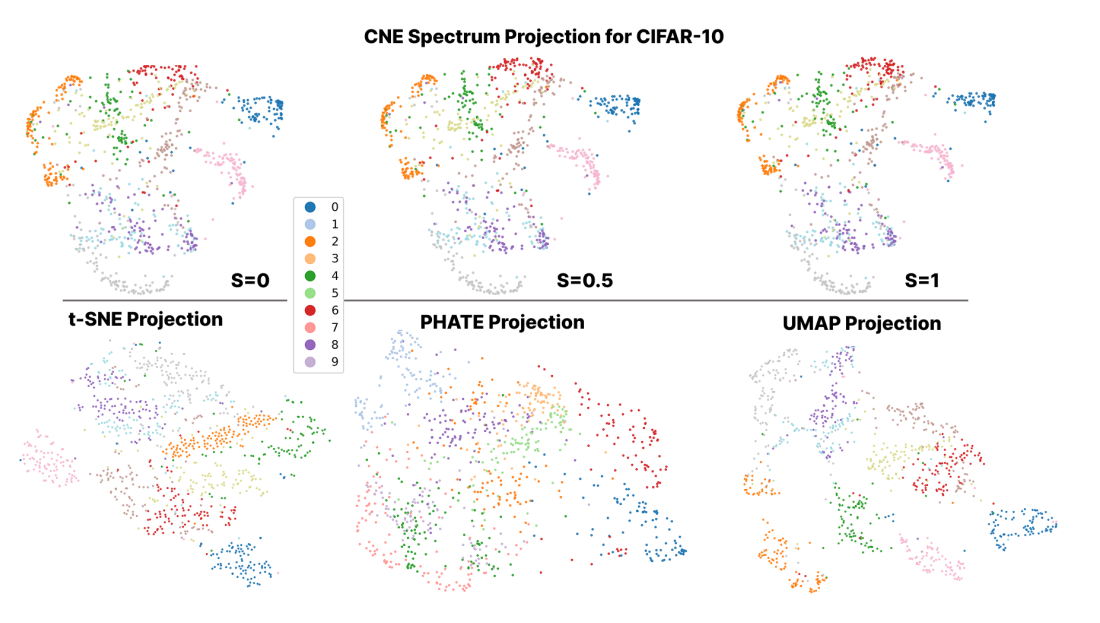


Figure 4: Pointwise setting: CIFAR-10 (1000 non-anchor points, 783 anchors)

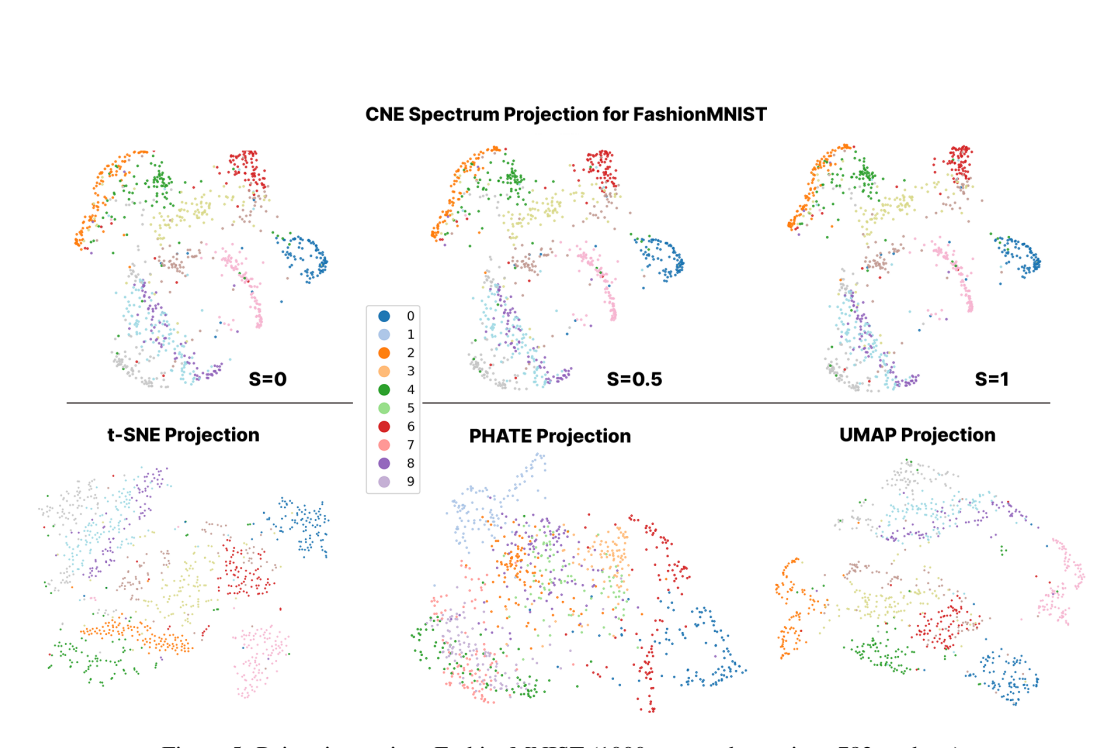


Figure 5: Pointwise setting: FashionMNIST (1000 non-anchor points, 783 anchors)

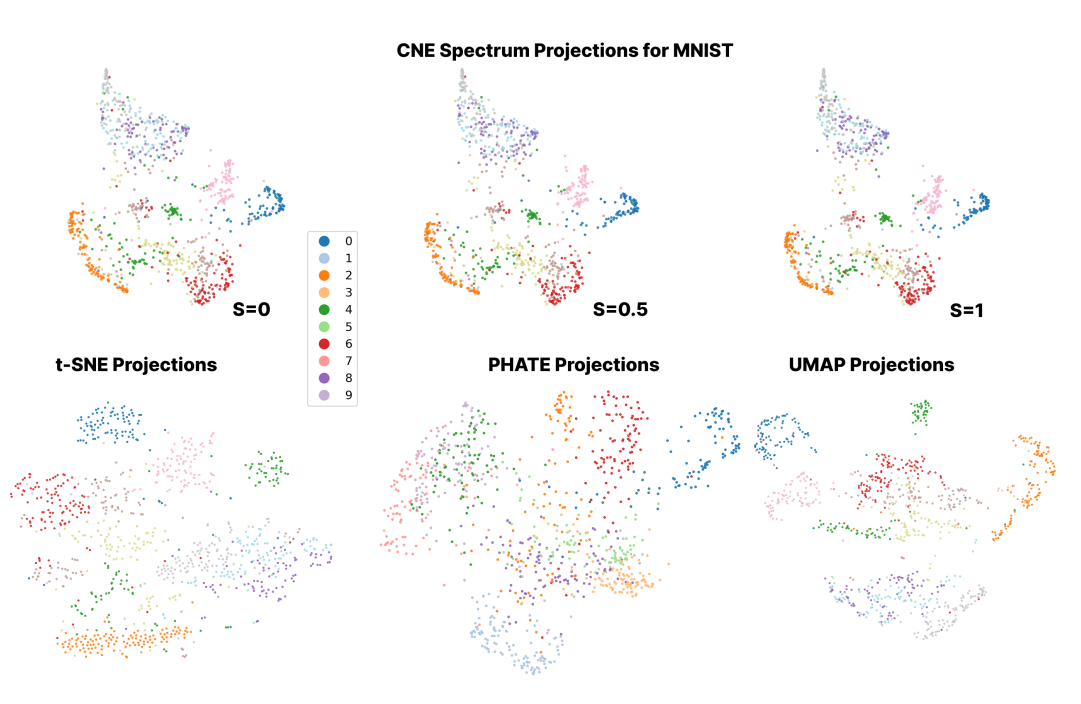


Figure 6: Pointwise setting: MNIST (1000 non-anchor points, 783 anchors)

A.15 RESULTS.

Table 8: FS and DE across IID, and non-IID balanced and unbalanced splits.

Data]	IID]	Bal	Unbal			
	FS	DE	FS	DE	FS	DE		
PNEU.	0.92	0.0052	0.87	0.0066	0.91	0.0055		
BLOOD	0.90	0.0052	0.89	0.0051	0.90	0.0052		
BREAST	0.95	0.0092	0.92	0.0113	0.91	0.0124		
DERMA	0.96	0.0029	0.93	0.0031	0.96	0.0029		
RETINA	0.96	0.0221	0.94	0.0272	0.96	0.0214		
ORGANC	0.80	0.0092	0.79	0.0089	0.79	0.0092		
ORGANS	0.81	0.0089	0.80	0.0085	0.81	0.0093		
GERMAN	0.75	0.0565	0.73	0.0621	0.72	0.0629		

Table 9: FS and DE under POINTWISE, IID, and NON-IID settings, comparing MULTISITE-FULL and MULTISITE-PARTIAL.

Dataset	Pointwise		IID-Full		IID-P	artial	Non-II	D-Full	Non-IID-Partial		
	FS	DE	FS	DE	FS	DE	FS	DE	FS	DE	
MNIST	0.9557	0.0057	0.8034	0.0097	0.9266	0.0438	0.7864	0.0101	0.9275	0.0434	
FashionMNIST	0.9560	0.0058	0.7586	0.0070	0.8726	0.0153	0.7534	0.0070	0.8754	0.0156	
CIFAR-10	0.9562	0.0057	0.9303	0.0049	0.9277	0.0044	0.9308	0.0049	0.9380	0.0044	

Table 10: Multisite setting comparison Non-iid unbalanced: Full vs Partial: Evaluation of different methods (Vanilla and SENSE variants) across different metrics.

Data	Metric	t-S	NE	UM	IAP	PH	ATE	CNE	(s=0)	CNE((s=0.5)	CNE	2(s=1)
		VAN.	SENSE	VAN.	SENSE	VAN.	SENSE	VAN.	SENSE	VAN.	SENSE	VAN.	SENSE
	— Multisite-Partial Setting —												
	Trust.	0.9259	0.9274	0.7447	0.7476	0.8175	0.8174	0.8334	0.8336	0.8322	0.8321	0.8232	0.8244
CIFAR-10	Cont.	0.9107	0.9391	0.8756	0.8804	0.9369	0.9381	0.9554	0.9552	0.9552	0.9549	0.9565	0.9561
CITAK-10	Stead.	0.8099	0.8165	0.6904	0.6938	0.7363	0.7349	0.7609	0.7654	0.7619	0.7580	0.7415	0.7487
	Cohes.	0.4707	0.4806	0.3725	0.3752	0.4927	0.4857	0.4708	0.4630	0.4716	0.4778	0.4766	0.4793
— Multisite-Full Setting —													
	Trust.	0.9259	0.9270	0.7447	0.7482	0.8175	0.8168	0.8334	0.8336	0.8322	0.8329	0.8232	0.8247
CIFAR-10	Cont.	0.9107	0.9364	0.8756	0.8808	0.9369	0.9366	0.9554	0.9553	0.9552	0.9550	0.9565	0.9561
CITAK-10	Stead.	0.8099	0.8229	0.6904	0.6875	0.7363	0.7357	0.7609	0.7624	0.7619	0.7580	0.7415	0.7464
	Cohes.	0.4707	0.4673	0.3725	0.3674	0.4927	0.4831	0.4708	0.4662	0.4716	0.4690	0.4766	0.4811
					— Poi	ntwise-Fu	ıll Setting	_					
	Trust.	0.9683	0.9659	0.9435	0.9419	0.8488	0.8531	0.9112	0.9123	0.9082	0.9079	0.9021	0.9035
	Cont.	0.9465	0.9448	0.9379	0.9333	0.9533	0.9527	0.9446	0.9442	0.9458	0.9437	0.9445	0.9442
CIFAR-10	Stead.	0.8061	0.8081	0.7793	0.7825	0.7111	0.7165	0.7992	0.7878	0.7887	0.8005	0.7808	0.7920
CIFAR-10	Cohes.	0.7482	0.7672	0.7415	0.7336	0.7431	0.7365	0.7485	0.7451	0.7513	0.7473	0.7435	0.7350

A.16 DISCUSSION.

SENSE in Evolving Distributed Environments. In dynamic settings, new data points arrive continuously e.g., a hospital admitting a patient, a bank processing a transaction, or a platform onboarding a user. Recomputing the full embedding for each arrival is inefficient and may disrupt global structure. Existing decentralized NE methods (Li et al., 2024; Qiao et al., 2024; Saha et al., 2017; Saha et al.) assume static datasets and lack support for incremental updates, making them unsuitable for streaming environments. SENSE, by contrast, is modular and compatible with out-of-sample embedding methods (Herath et al., 2021; Bengio et al., 2003; Oster et al., 2021). Once the global embedding is constructed via anchor-based completion and NE optimization, it defines a geometry-aware coordinate space that supports new points without full recomputation. Let $\mathbf{X}_{NA} = [\mathbf{x}_1, \dots, \mathbf{x}_N] \in \mathbb{R}^{N \times d_h}$ be the reconstructed NA embeddings. When a new point \mathbf{y} arrives, we select K existing points as pseudo-anchors $\mathcal{A} = \{a_1, \dots, a_K\} \subset \mathbf{X}_{NA}$, with coordinates $\mathbf{X}_A = [\mathbf{p}_1, \dots, \mathbf{p}_K]^{\top} \in \mathbb{R}^{K \times d_h}$. Given dissimilarities $\{\delta_{l_i y}\}_{i=1}^K$ to these anchors, we compute the embedding $\hat{\mathbf{y}}$ by solving:

$$\hat{\sigma}(\hat{\mathbf{y}}) = \sum_{i=1}^{K} (\|\mathbf{p}_i - \hat{\mathbf{y}}\|_2 - \delta_{l_i y})^2.$$
 (23)

Table 11: IID setting: Evaluation of different dimensionality reduction methods (Vanilla and SENSE variants) across various metrics.

Data	Metric	t-S	NE	UN	IAP	PH	ATE	CNE	(s=0)	CNE(s=0.5)	CNE	(s=1)
		VAN.	SENSE										
	Trust.	0.9718	0.9700	0.7687	0.7700	0.8573	0.8590	0.9016	0.9026	0.8973	0.8967	0.8837	0.8795
	Cont.	0.9395	0.9442	0.9145	0.9143	0.9616	0.9598	0.9592	0.9587	0.9591	0.9582	0.9606	0.9598
D : MATTOR	Stead.	0.7840	0.7844	0.6203	0.6272	0.7158	0.7228	0.7554	0.7516	0.7439	0.7424	0.7369	0.7263
PneumoniaMNIST	Cohes.	0.7031	0.6963	0.6081	0.6272	0.6902	0.6898	0.7013	0.7112	0.6981	0.6970	0.7006	0.7050
	Trust.	0.9628	0.9611	0.8643	0.8633	0.8515	0.8527	0.8847	0.8820	0.8793	0.8820	0.8729	0.8736
	Cont.	0.9312	0.9280	0.9416	0.9391	0.9444	0.9440	0.9555	0.9558	0.9556	0.9558	0.9553	0.9556
BloodMNIST	Stead.	0.7515	0.7436	0.6899	0.6764	0.6967	0.6871	0.7259	0.7211	0.7228	0.7211	0.7164	0.7133
BIOOGMINIST	Cohes.	0.7085	0.7106	0.7233	0.7261	0.7416	0.7469	0.7435	0.7339	0.7329	0.7339	0.7453	0.7462
	Trust.	0.9382	0.9370	0.7599	0.7589	0.8835	0.8774	0.8938	0.8924	0.8939	0.8920	0.8934	0.8924
	Cont.	0.9452	0.9412	0.8147	0.8174	0.9533	0.9526	0.9450	0.9446	0.9450	0.9445	0.9450	0.9444
BreastMNIST	Stead.	0.8522	0.8514	0.5800	0.5697	0.8056	0.8099	0.8400	0.8400	0.8287	0.8308	0.8317	0.8353
Breasuviinis i	Cohes.	0.6028	0.5987	0.4226	0.4226	0.5639	0.5611	0.5566	0.5605	0.5637	0.5670	0.5532	0.5606
	Trust.	0.9758	0.9762	0.7513	0.7480	0.8726	0.8726	0.9129	0.9118	0.9125	0.9126	0.9017	0.9023
	Cont.	0.9592	0.9583	0.9134	0.9129	0.9736	0.9729	0.9709	0.9712	0.9707	0.9706	0.9716	0.9714
DermaMNIST	Stead.	0.7995	0.7976	0.5930	0.5945	0.7332	0.7291	0.7726	0.7739	0.7694	0.7638	0.7580	0.7577
Definalvirvisi	Cohes.	0.7294	0.7107	0.5590	0.5618	0.7001	0.7184	0.7339	0.7334	0.7390	0.7373	0.7308	0.7297
	Trust.	0.9797	0.9758	0.8777	0.8643	0.9144	0.9038	0.9480	0.9335	0.9469	0.9331	0.9450	0.9313
	Cont.	0.9669	0.9567	0.9280	0.9232	0.9738	0.9730	0.9718	0.9711	0.9704	0.9700	0.9678	0.9678
RetinaMNIST	Stead.	0.8483	0.8479	0.6120	0.5941	0.7618	0.7434	0.8183	0.8140	0.8117	0.8050	0.8105	0.8086
Kennaminisi	Cohes.	0.7051	0.6963	0.5835	0.5515	0.6980	0.6995	0.7123	0.7074	0.7046	0.7112	0.6831	0.7135
	Trust.	0.9608	0.9482	0.8879	0.8815	0.8845	0.8858	0.9149	0.9028	0.9160	0.9039	0.9024	0.8890
	Cont.	0.9238	0.9413	0.9231	0.9242	0.9696	0.9682	0.9731	0.9683	0.9730	0.9679	0.9738	0.9688
OrganCMNIST	Stead.	0.6948	0.8027	0.7575	0.7678	0.7994	0.8058	0.8690	0.8677	0.8788	0.8673	0.8624	0.8593
Organiciviivisi	Cohes.	0.4762	0.4849	0.3335	0.3145	0.5695	0.5153	0.4751	0.4760	0.5268	0.5001	0.5545	0.5166
	Trust.	0.9565	0.9421	0.8707	0.8588	0.8766	0.8890	0.9130	0.9026	0.9128	0.9034	0.8991	0.8911
	Cont.	0.9219	0.9366	0.9248	0.9211	0.9679	0.9717	0.9741	0.9684	0.9732	0.9672	0.9737	0.9679
OrganSMNIST	Stead.	0.6793	0.7753	0.7305	0.7513	0.7786	0.7965	0.8609	0.8691	0.8649	0.8745	0.8517	0.8601
Organion 11101	Cohes.	0.4856	0.4702	0.3327	0.3316	0.5575	0.5094	0.4838	0.4525	0.5312	0.4889	0.5564	0.4783
	Trust.	0.9771	0.9553	0.9505	0.9330	0.8559	0.8551	0.9380	0.9224	0.9359	0.9140	0.9325	0.9192
	Cont.	0.9590	0.9434	0.9587	0.9449	0.9482	0.9294	0.9573	0.9448	0.9573	0.9429	0.9564	0.9432
german-credit	Stead.	0.8603	0.8251	0.8342	0.7907	0.7500	0.7228	0.8414	0.7954	0.8416	0.7883	0.8401	0.7944
50ian crean	Cohes.	0.6810	0.6895	0.6542	0.6413	0.6712	0.6640	0.6465	0.6651	0.6577	0.6675	0.6624	0.6550

Table 12: Non-IID (balanced) setting: Evaluation of different methods (Vanilla and SENSE variants) across different metrics.

Data	Metric	t-S	NE	UN	IAP	PH	ATE	CNE	(s=0)	CNE(s=0.5)	CNE	(s=1)
		VAN.	SENSE										
	Trust.	0.9566	0.9483	0.8806	0.8658	0.8909	0.8937	0.9430	0.9393	0.9372	0.9343	0.9226	0.9168
	Cont.	0.9228	0.9278	0.9031	0.9114	0.9776	0.9732	0.9683	0.9678	0.9690	0.9686	0.9704	0.9695
PneumoniaMNIST	Stead.	0.6952	0.7165	0.6007	0.6211	0.7146	0.7244	0.7778	0.7737	0.7694	0.7692	0.7622	0.7579
FileumomawiNiSi	Cohes.	0.6377	0.6815	0.6205	0.6070	0.6650	0.6771	0.7259	0.7162	0.7240	0.7145	0.7172	0.7336
	Trust.	0.9304	0.9292	0.8902	0.8796	0.8640	0.8633	0.9003	0.8972	0.8959	0.8944	0.8862	0.8856
	Cont.	0.9020	0.9029	0.9385	0.9390	0.9510	0.9492	0.9618	0.9611	0.9620	0.9614	0.9622	0.9614
BloodMNIST	Stead.	0.7060	0.7017	0.6815	0.6927	0.6812	0.6927	0.7531	0.7505	0.7466	0.7442	0.7536	0.7395
DIOOGIVINIST	Cohes.	0.6781	0.6761	0.7210	0.7096	0.7620	0.7540	0.7441	0.7603	0.7472	0.7335	0.7561	0.7603
	Trust.	0.9643	0.9657	0.8476	0.8562	0.9188	0.9241	0.9403	0.9422	0.9385	0.9418	0.9383	0.9415
	Cont.	0.9632	0.9658	0.8567	0.8408	0.9587	0.9671	0.9604	0.9594	0.9598	0.9590	0.9599	0.9591
BreastMNIST	Stead.	0.8331	0.8370	0.5159	0.5081	0.7585	0.7913	0.8712	0.8742	0.8684	0.8616	0.8691	0.8675
Dicastiviivisi	Cohes.	0.6174	0.6018	0.3677	0.3741	0.5187	0.5165	0.5254	0.5667	0.5265	0.5413	0.5200	0.5485
	Trust.	0.9545	0.9467	0.8253	0.8048	0.8963	0.8961	0.9335	0.9351	0.9292	0.9327	0.9147	0.9167
	Cont.	0.9403	0.9284	0.8977	0.8895	0.9825	0.9815	0.9742	0.9734	0.9743	0.9733	0.9761	0.9756
DermaMNIST	Stead.	0.7304	0.7148	0.5608	0.5428	0.7327	0.7295	0.7901	0.7909	0.7834	0.7841	0.7751	0.7743
Defination	Cohes.	0.6493	0.6484	0.5159	0.5152	0.6867	0.6726	0.6993	0.6976	0.6976	0.7128	0.6902	0.7012
	Trust.	0.9749	0.9743	0.8933	0.8829	0.9228	0.9227	0.9522	0.9523	0.9492	0.9519	0.9497	0.9495
	Cont.	0.9627	0.9616	0.9289	0.9152	0.9752	0.9729	0.9720	0.9713	0.9712	0.9700	0.9670	0.9675
RetinaMNIST	Stead.	0.8447	0.8380	0.6155	0.6174	0.7534	0.7559	0.8224	0.8172	0.8134	0.8189	0.8123	0.8046
Technalyn vio i	Cohes.	0.7140	0.7283	0.5785	0.5648	0.7189	0.6836	0.7292	0.7005	0.7092	0.6938	0.7039	0.6849
	Trust.	0.9489	0.9271	0.8975	0.8888	0.9005	0.8984	0.9235	0.9132	0.9232	0.9126	0.9140	0.8994
	Cont.	0.9210	0.9082	0.9232	0.9185	0.9737	0.9719	0.9756	0.9715	0.9750	0.9710	0.9760	0.9717
OrganCMNIST	Stead.	0.6365	0.7142	0.7462	0.7290	0.8038	0.7909	0.8611	0.8724	0.8660	0.8745	0.8621	0.8640
Organiciviivisi	Cohes.	0.4862	0.4913	0.3249	0.3191	0.5088	0.5154	0.5338	0.4980	0.5266	0.4974	0.4908	0.5282
	Trust.	0.9383	0.9093	0.8954	0.8861	0.9054	0.9071	0.9269	0.9190	0.9291	0.9194	0.9172	0.9092
	Cont.	0.9164	0.8881	0.9168	0.9255	0.9774	0.9758	0.9796	0.9746	0.9786	0.9741	0.9788	0.9741
OrganSMNIST	Stead.	0.5896	0.6154	0.6315	0.6953	0.7784	0.7963	0.8591	0.8684	0.8560	0.8634	0.8411	0.8523
Organisiviivisi	Cohes.	0.5109	0.5108	0.3441	0.3665	0.5642	0.5278	0.5079	0.4878	0.5461	0.5021	0.5487	0.5001
·	Trust.	0.9752	0.9575	0.9511	0.9301	0.8552	0.8508	0.9403	0.9211	0.9380	0.9172	0.9350	0.9176
	Cont.	0.9581	0.9418	0.9606	0.9427	0.9481	0.9240	0.9576	0.9470	0.9575	0.9463	0.9571	0.9460
german-credit	Stead.	0.8567	0.8267	0.8350	0.7850	0.7398	0.7023	0.8484	0.8063	0.8475	0.8016	0.8405	0.8020
german-creun	Cohes.	0.6795	0.6837	0.6488	0.6509	0.6870	0.6828	0.6620	0.6834	0.6557	0.6676	0.6564	0.6653

Here, $\delta_{l_i y}$ is the dissimilarity in the original space, and $\|\mathbf{p}_i - \hat{\mathbf{y}}\|_2$ is the distance in the embedding space. Only $\hat{\mathbf{y}}$ is optimized, anchors remain fixed. Since $K < d_h$, exact recovery is impossible (Theorems 3.1, 3.2), ensuring privacy. This lightweight optimization requires no raw data and supports real-time integration, making SENSE well-suited for scalable, privacy-constrained systems.

Scalability and Computational Complexity. In addition to the 14 standard DR datasets (Sec. 4.1), we evaluate SENSE on two large-scale benchmarks: Tiny ImageNet (Le & Yang, 2015) (\sim 90k NAs, with 512D features extracted using an ImageNet-pretrained ResNet-34 (He et al., 2016)) and Street View House Numbers (Netzer et al., 2011) (SVHN, \sim 80k NAs, $d_h = 512$). These experiments are conducted for *Multisite setting*, where we distributed the NA samples to 10 clients in non-IID unbalanced scenarios. Results in Table 13 demonstrate that SENSE maintains strong performance even at this scale, with runtimes of only \sim 12–14 seconds per iteration.

Table 13: SENSE performance compared to DR baselines on Tiny ImageNet and SVHN. Runtime is averaged per iteration.

Data	Metric	t-SNE VAN	SENSE	UMAP VAN	SENSE	PHATE VAN	SENSE	CNE(0) VAN	SENSE	CNE(0.5) VAN	SENSE	CNE(1) VAN	SENSE	Runtime
TinyImageNet	Trust Cont Stead Cohes	0.9245 0.9107 0.8099 0.7680	0.9341 0.9064 0.8229 0.7548	0.7748 0.9334 0.5703 0.8305	0.7330 0.9140 0.5755 0.6685	0.7480 0.9359 0.5550 0.8340	0.7392 0.9029 0.6248 0.7439	0.7682 0.9396 0.5848 0.8344	0.7402 0.9268 0.6205 0.7223	0.7960 0.9350 0.5986 0.8296	0.7637 0.9244 0.6298 0.7160	0.7717 0.9411 0.5807 0.8403	0.7467 0.9294 0.6135 0.7322	13.72s
SVHN	Trust Cont Stead Cohes	0.9822 0.9619 0.7234 0.8362	0.9801 0.9630 0.7200 0.8349	0.8973 0.9749 0.6545 0.8430	0.8914 0.9701 0.6664 0.7160	0.8825 0.9759 0.6426 0.8544	0.8819 0.9665 0.6739 0.7834	0.8910 0.9778 0.6540 0.8503	0.8900 0.9745 0.6968 0.7935	0.9033 0.9787 0.6705 0.8493	0.9068 0.9648 0.7027 0.6960	0.8939 0.9787 0.6556 0.8576	0.8964 0.9646 0.7134 0.7535	13.50s

We also provide detailed runtime and complexity analysis. With N NA points and K anchors, Anchored-MDS in Sec 2 has complexity $\mathcal{O}(K^2d_h + KNd_h)$, efficient as $K \ll N$ and $K < d_h$ (for privacy). We use the fastest variants of different global low-dimensional embedding methods in our framework, as this is the second stage in the pipeline. Notation: here k denotes the number of neighbors considered per point (in the attractive force calculation), d_h is the embedding dimension, n are the number of data points (samples) and m are the number of negative (repulsive) samples per positive interaction. 1) Fast NE methods: Van-t-SNE takes $\mathcal{O}(n^2d_h)$ (van der Maaten & Hinton, 2008), Barnes-Hut t-SNE (BH-t-SNE) and FIt-SNE (FFT-based interpolation) takes $\mathcal{O}(kn\log n \cdot 2^{d_h})$ and $\mathcal{O}(kn \cdot 2^{d_h})$ respectively. 2) The contrastive neighbor embedding: These methods only sample nm repulsive interactions per epoch (instead of all pairs) with complaexity $\mathcal{O}(kmnd_h)$, which scales linearly with embedding dimension d_h . This also includes NC-t-SNE/UMAP with contrastive loss runs in $\mathcal{O}(kmd_h)$ with $m \ll n$ repulsive samples per epoch (Damrich et al., 2023).

We also provide empirical results on the different stages of the pipeline. Table 14 reports empirical results for individual stages of the SENSE pipeline.

Table 14: Runtime for SENSE pipeline stages: stage1 = incomplete matrix, stage2 = matrix completion.

Data	NA	K	Stage1(s)	Stage2(s)	Total(s)	FS	DE
BloodMNIST	1k	100	0.33	2.22	2.55	0.86	0.02
		1k	0.34	8.11	8.45	0.94	0.01
	5k	100	0.46	39.33	39.79	0.81	0.00
	2k	50	0.59	54.83	55.42	0.92	0.01

Curated Privacy Example. To illustrate the privacy guarantees of SENSE, we constructed a curated dataset containing sensitive attributes (e.g., age) and categorical features (e.g., gender, occupation). The setup involves five clients (C_1-C_5) , each with five attributes (d=5), and four reference anchors (K=4 < d). Embeddings are computed exclusively from client–anchor distances, without direct access to raw features. As shown in Table 15, the resulting embeddings preserve structural relationships while preventing recovery of private attributes, thereby empirically validating the privacy-preserving nature of SENSE.

Why SENSE Avoids Noise-Based Privacy. Noise injection is a common privacy mechanism, but SENSE is built on a different principle. The goal is not to obscure the distance map, but to

Table 15: Original private attributes vs. SENSE embeddings. Sensitive details are not exposed by the embeddings.

Original Data	x_1	x_2	x_3	x_4	x_5
C_1	1500	25	3	1	10
C_2	2000	35	2	0	15
C_3	1745	28	2	0	18
C_4	1620	32	1	1	13
C_5	1200	45	3	1	12
SENSE Emb	x_1	x_2	x_3	x_4	x_5
C_1	80.630	26.896	13.795	96.939	-39.321
C_2	-189.837	-28.557	-61.648	-272.603	141.184
C_3	-58.064	2.598	-26.164	-79.338	49.985
C_4	-5.492	-2.856	6.935	12.915	-12.891
C_5	210.016	14.741	75.140	328.458	-172.165

preserve inter-client similarity while ensuring that high-dimensional raw features remain private. In this setting, noise-based privacy is problematic for two reasons. First, robustness to injected noise is inherently unreliable in decentralized DR, where incomplete similarity information amplifies perturbations. Second, our experiments show that even mild noise sharply degrades embedding quality, making noise-based approaches unstable and costly. We evaluated two scenarios: (i) noise added to client—anchor distance vectors, and (ii) Gaussian perturbations applied directly to raw features.

Empirical Evaluation 1: Noise Added to Anchor-NA Distance Vectors. We injected noise into the *F* block of Eq. 8, corresponding to client–anchor distances, under the *Pointwise* setting (each client has a single NA). A random fraction of clients was selected, and noise was added to their anchor distance vectors. Results on *Iris* and *Seeds* (Table 16) show a clear trade-off: as the fraction of noisy clients increases, F-score (FS) drops sharply while Distance Error (DE) rises, confirming the fragility of noise-based privacy in SENSE.

Table 16: Effect of noise injection into F matrix: FS decreases and DE increases as noise fraction increases.

Data	Metric	0%	5%	10%	20%	50%
Iris	FS	0.8659	0.8403	0.8104	0.7000	0.6167
	DE	0.0425	0.0735	0.0929	0.1528	0.1828
Seeds	FS	0.9745	0.9390	0.9038	0.7902	0.6589
	DE	0.0102	0.1251	0.1760	0.2471	0.3702

Empirical Evaluation 2: Noise to Raw Features. We also injected Gaussian noise directly into raw features (e.g., pixel-level perturbations on MNIST) using the *Multisite* setting of SENSE with $K = d_h$, 10 clients, and 100 NAs. In the noise-based variant (NS), element-wise zero-mean Gaussian noise with varying standard deviations (scaled to the data range) was applied. As shown in Table 17, even mild perturbations lead to sharp drops in FS and significant increases in DE, confirming that noise-based privacy comes at a substantial cost to utility compared with SENSE without noise. In real-world domains such as healthcare or finance, where precision is critical, this trade-off is unacceptable.

Table 17: Performance of SENSE versus noise-based variants (NS) with Gaussian perturbation of raw features.

Method	DE	FS		
SENSE	0.006023	0.974955		
NS1	0.074474	0.946197		
NS2	0.268156	0.887382		
NS3	0.535183	0.801178		
NS4	0.843552	0.691761		
NS5	1.175783	0.573909		

Across both evaluations, noise-based privacy consistently degraded utility without providing stronger guarantees. These findings highlight why SENSE achieves privacy not through artificial corruption, but through geometric underdetermination: the structure needed for downstream tasks is preserved, while raw features remain unrecoverable. In domains such as healthcare and finance, where precision is critical, this distinction makes noise-based privacy an impractical choice.